



1 **Near-surface and path-averaged mixing ratios of NO<sub>2</sub> derived**  
2 **from car DOAS zenith-sky and tower DOAS off-axis**  
3 **measurements in Vienna: a case study**

4 **Stefan F. Schreier<sup>1</sup>, Andreas Richter<sup>2</sup>, and John P. Burrows<sup>2</sup>**

5 <sup>1</sup>Institute of Meteorology, University of Natural Resources and Life Sciences, Vienna, Austria

6 <sup>2</sup>Institute of Environmental Physics, University of Bremen, Germany

7 Correspondence to: S. F. Schreier ([stefan.schreier@boku.ac.at](mailto:stefan.schreier@boku.ac.at))

8

9

10 **Abstract.** Nitrogen dioxide (NO<sub>2</sub>), produced as a result of fossil fuel combustion, biomass burning,  
11 lightning, and soil emissions, is a key urban and rural tropospheric pollutant. In this case study,  
12 ground-based remote sensing has been coupled with the in situ network in Vienna, Austria, to  
13 investigate NO<sub>2</sub> distributions in the planetary boundary layer. Near-surface and path-averaged NO<sub>2</sub>  
14 mixing ratios within the metropolitan area of Vienna are estimated from car DOAS (Differential  
15 Optical Absorption Spectroscopy) zenith-sky and tower DOAS horizon observations. The latter  
16 configuration is innovative in the sense that it obtains horizontal measurements at more than  
17 hundred different azimuthal angles – within a 360° rotation taking less than half an hour. Spectral  
18 measurements were made with a DOAS instrument on nine days in April, September, October, and  
19 November 2015 in the zenith-sky mode and on five days in April and May 2016 in the off-axis  
20 mode. The analysis of tropospheric NO<sub>2</sub> columns from the car measurements and O<sub>4</sub> normalized  
21 NO<sub>2</sub> path averages from the tower observations provide interesting insights into the spatial and  
22 temporal NO<sub>2</sub> distribution over Vienna. Integrated column amounts of NO<sub>2</sub> from both DOAS-type  
23 measurements are converted into mixing ratios by different methods. The estimation of near-  
24 surface NO<sub>2</sub> mixing ratios from car DOAS tropospheric NO<sub>2</sub> vertical columns is based on a linear  
25 regression analysis including mixing-height and other meteorological parameters that affect the  
26 dilution and reactivity in the planetary boundary layer – a new approach for such conversion. Path-



1 averaged NO<sub>2</sub> mixing ratios are calculated from tower DOAS NO<sub>2</sub> slant column densities by taking  
2 into account topography and geometry. Overall, lap averages of near-surface NO<sub>2</sub> mixing ratios  
3 obtained from car DOAS zenith-sky measurements, around a circuit in Vienna, are in the range of  
4 3.8 to 26.2 ppb and in good agreement with values obtained from in situ NO<sub>2</sub> measurements for  
5 days with wind from the Southeast. Path-averaged NO<sub>2</sub> mixing ratios at 160 m above the ground  
6 as derived from the tower DOAS measurements are between 2.5 and 9 ppb on two selected days  
7 with different wind conditions and pollution levels and show similar spatial distribution as seen in  
8 the car DOAS zenith-sky observations. We conclude that the application of the two methods to  
9 obtain near-surface and path-averaged NO<sub>2</sub> mixing ratios is promising for this case study.

10

## 11 **1 Introduction**

12 Tropospheric nitrogen oxides (NO<sub>x</sub> = NO + NO<sub>2</sub>) are released from various human activities and  
13 natural sources (Lee et al., 1997). Fossil fuel combustion to produce energy results in NO<sub>x</sub>  
14 emissions by traffic, industry and domestic heating or cooling appliances. Nitric oxide (NO) is the  
15 predominant part of NO<sub>x</sub> emitted from these sources. However it is rapidly converted to nitrogen  
16 dioxide (NO<sub>2</sub>) by reaction with ozone (O<sub>3</sub>). During daytime, given sufficient ultraviolet radiation,  
17 NO<sub>2</sub> is photolysed to produce NO and oxygen atoms. The reaction of oxygen atoms with molecular  
18 oxygen (O<sub>2</sub>) results in the production of O<sub>3</sub>. Under polluted conditions the so called Leighton  
19 photostationary state is established. However, as the NO<sub>x</sub> air is mixed in daylight with  
20 hydrocarbons and being diluted, the catalytic production of O<sub>3</sub> results and nitric acid (HNO<sub>3</sub>) is  
21 formed. The latter is absorbed on aerosols, which are also produced in air masses generating  
22 photochemical smog.

23 Although NO<sub>x</sub> concentrations are relatively low in the atmosphere, these reactive gases play a  
24 significant role in atmospheric chemistry, air pollution, and climate change, in particular in urban  
25 environments (e.g. WHO, 2003; IPCC, 2013). For example, elevated levels of air pollutants such  
26 as NO<sub>2</sub> and O<sub>3</sub> affect human health (e.g. Dockery et al., 1993), as the long-term exposure to these  
27 gases can influence mortality and morbidity (e.g. Künzli et al., 2000).



1 In addition to the in situ NO<sub>2</sub> measurement techniques such as chemiluminescence monitors (e.g.  
2 Fontijn et al., 1970), the differential optical absorption spectroscopy (DOAS) method (Perner and  
3 Platt, 1979) can also be used to quantify atmospheric NO<sub>2</sub> concentrations. Nowadays, the DOAS  
4 technique is a widely-used remote sensing method to retrieve the amount of several trace gases  
5 having narrow band absorption structures in the UV and visible part of the electromagnetic  
6 spectrum. The (passive) DOAS principle, which is based on Lambert-Beer's law, can be applied to  
7 measurements from various ground-based, ship-based, aircraft-based, and satellite-based platforms  
8 (e.g. Platt and Stutz, 2008 and references therein).

9 The great advantage of satellite-based measurements is their daily (near) global coverage and thus,  
10 the possibility to evaluate temporal trends above selected regions. However, it is difficult to resolve  
11 NO<sub>2</sub> at the city scale because of the coarse resolution of satellite sensors (Richter et al., 2005;  
12 Hilboll et al., 2013). Aircraft-based measurements deliver higher resolved images of the spatial  
13 NO<sub>2</sub> distribution along a given flight track, but only during short-term measurement campaigns  
14 (Heue et al., 2005; Wang et al., 2005; Schönhardt et al., 2015; Meier et al., 2017; Nowlan et al.,  
15 2018). As is the case for aircraft-based DOAS measurements of NO<sub>2</sub>, ship-based observations of  
16 NO<sub>2</sub> are also usually performed on a campaign basis (Peters et al., 2012; Takashima et al., 2012;  
17 Schreier et al., 2015; Hong et al., 2018). Finally, information on tropospheric NO<sub>2</sub> can also be  
18 obtained from ground-based platforms using the Multi AXis (MAX) DOAS system (Hönninger et  
19 al., 2004; Wittrock et al., 2004). In contrast to other platforms, ground-based DOAS measurements  
20 are usually performed continuously and at fixed locations.

21 More recently, DOAS-type measurements of NO<sub>2</sub> are also performed from a car, which enables  
22 the observation of the horizontal variation of tropospheric NO<sub>2</sub>, in addition to its temporal  
23 evolution. Such observations have been used for the quantification of total emissions from cities  
24 and/or known emission sources (Johansson et al., 2008; Rivera et al., 2009; Ibrahim et al., 2010;  
25 Shaiganfar et al., 2011; Wang et al., 2012; Frins et al., 2014; Ionov et al., 2015), for the estimation  
26 of emission fluxes from cities (Johansson et al., 2009; Rivera et al., 2013), for the comparison with  
27 satellite observations of NO<sub>2</sub> (Wagner et al., 2010; Constantin et al., 2013; Wu et al., 2013), for the  
28 comparison with model simulations (Dragomir et al., 2015), and for the validation of airborne  
29 measurements of NO<sub>2</sub> (Meier et al., 2017; Tack et al., 2017; Merlaud et al., 2018). While some of  
30 the mentioned studies use the MAX-DOAS measurement principle, others apply their instruments



1 in the zenith-sky viewing mode only. The main challenges for the retrieval of tropospheric NO<sub>2</sub> for  
2 the latter approach are obtaining accurate knowledge of the NO<sub>2</sub> signal in the reference  
3 measurement as well as the removal of the stratospheric NO<sub>2</sub> contribution (as a function of SZA).  
4 Both quantities cannot directly be separated from the zenith-sky measurements alone and thus, not  
5 accounting for these contributions can lead to large errors, especially in regions with low NO<sub>2</sub>  
6 levels (Wagner et al. 2010). Therefore, approaches were developed to estimate these contributions  
7 by using additional data and methods. While the stratospheric NO<sub>2</sub> amounts can be obtained from  
8 satellite measurements in combination with atmospheric modelling, the background signal in the  
9 reference spectrum can be estimated by calculating a reference measurement applying the Langley-  
10 plot method (Constantin et al. 2013). Another approach to estimate the background signal in the  
11 reference spectrum would be to utilize NO<sub>2</sub> concentration measurements from nearby in situ  
12 monitoring stations and convert those quantities into tropospheric NO<sub>2</sub> vertical columns, e.g. by  
13 applying an empirical relationship (Kramer et al., 2008).

14 The aims of the present study are two-fold. Firstly, it attempts to build on earlier work and  
15 investigates the spatial and temporal variability of NO<sub>2</sub> pollution in Vienna by using a simple  
16 zenith-sky telescope and a miniature spectrometer operated from a normal car. The relatively large  
17 number of air quality monitoring stations in and around Vienna, including continuous  
18 measurements of NO<sub>2</sub> concentrations at surface level, provides the prerequisites for a comparison  
19 between these two observation systems which has not yet been performed in past studies. Secondly,  
20 the potential of DOAS horizon measurements, performed with the same instrument on a rotating  
21 tower platform in Vienna is investigated – a DOAS-type approach to gain detailed horizontal NO<sub>2</sub>  
22 distributions on the city-scale within less than half an hour. Our tower DOAS off-axis observations  
23 can be best compared to the measurement configuration of the CU 2-D-MAX-DOAS instrument  
24 during the Multi-Axis DOAS Comparison campaign for Aerosols and Trace gases (MAD-CAT) in  
25 Mainz, Germany (Ortega et al., 2015). The authors of that study developed a four-step retrieval to  
26 derive, amongst other parameters, near-surface horizontal distributions of NO<sub>2</sub> at 14 pre-set  
27 azimuth angles distributed over a 360° view. The tower DOAS off-axis configuration presented in  
28 our study is in the sense innovative that it is the first approach having more than 100 horizontal  
29 measurements within a 360° rotation that lasts less than half an hour. Also new is the performance  
30 of the DOAS instrument at an altitude of more than 100 meters above ground, which gives insights



1 into the vertical variability of NO<sub>2</sub> within the planetary boundary layer over the urban environment  
2 of Vienna, when these measurements are combined with ground-based in situ data. The horizontal  
3 optical path lengths in our study are estimated by making use of the combination of geometry and  
4 topography. We note that the discussion of tower DOAS off-axis measurements is only based on a  
5 couple of data available. Further measurements on a routine base could serve as a data set to go  
6 more in detail and estimate the 3-D distribution of trace gases, as shown in Ortega et al. (2015).

7 From both DOAS-type columnar NO<sub>2</sub> measurements reported in our study, near-surface and path-  
8 averaged NO<sub>2</sub> mixing ratios are estimated by using both existing methods and a novel linear  
9 regression analysis. These measurements provide insights about the NO<sub>2</sub> distributions in the  
10 Viennese boundary layer, which are interestingly in themselves but could also help in deciding  
11 where to place an optimal set of MAX-DOAS instruments around the capital and largest city of  
12 Austria. The proposed long-term measurements of these instruments, which are foreseen in the  
13 VINDOBONA (VIenna horizontal aNd vertical Distribution OBServations Of Nitrogen dioxide  
14 and Aerosols) project ([www.doas-vindobona.at](http://www.doas-vindobona.at)), will provide a valuable data set for analyzing the  
15 temporal variability of air pollutants over Vienna.

16 The city of Vienna has the second largest number of inhabitants (about 1.8 million) within German  
17 speaking countries. It is part of a metropolitan area having a population of 2.8 million and is a  
18 typical example of a growing city ([www.statistik.at](http://www.statistik.at)). There are many NO<sub>x</sub> emission sources such  
19 as high-traffic roads, individual power plants, and industrial buildings that contribute to increased  
20 levels of NO<sub>2</sub>. The Environment Agency Austria reported a significant decrease in NO<sub>x</sub> emissions  
21 from traffic and industry since 2005 in Austria, which is mainly because of the progress in  
22 automotive technology. However, they also highlighted the fact that a defined legal limit of annual  
23 mean NO<sub>2</sub> concentrations (35 µg/m<sup>3</sup>) was still exceeded in the past years at several Austrian air  
24 quality monitoring stations – including stations in Vienna (Spangl and Nagl, 2016). In the year  
25 2015, annual mean NO<sub>2</sub> concentrations exceeded the legal limit at one station in Vienna. Moreover,  
26 hourly limit values (200 µg/m<sup>3</sup>) were exceeded several times at four stations. We note that NO<sub>2</sub>  
27 levels didn't exceed the legal limits on the days of measurements presented in this case study.  
28 However, a substantial number of hourly values with NO<sub>2</sub> concentrations higher than 100 µg/m<sup>3</sup>  
29 were observed on these days.



1 In the following Sect. 2, the DOAS instrument and the setups for the car DOAS zenith-sky and  
2 tower DOAS off-axis measurements are introduced. Details about the data analysis, including the  
3 retrieval of columnar tropospheric NO<sub>2</sub> amounts and the conversion into mixing ratios are given in  
4 Sect. 3. The results of this study are described and discussed in Sect. 4, followed by a short  
5 summary and outlook (Sect. 5).

6

## 7 **2 Instrument and car journeys**

### 8 **2.1 DOAS instrument**

9 For the car DOAS zenith-sky and tower DOAS off-axis observations of tropospheric NO<sub>2</sub> in  
10 Vienna, a DOAS system was used to measure scattered sunlight from directly overhead and from  
11 the horizon, respectively. A cardboard box was built to house a commercial Avantes miniature  
12 spectrometer (AvaSpec-ULS2048x64) and a notebook. The AvaSpec-ULS2048x64 is small in size  
13 (175 x 110 x 44 mm), robust, and lightweight (855 grams). The instrument performs spectral  
14 measurements between 290 and 550 nm at a spectral resolution of 0.65 nm. Both the spectrometer  
15 and notebook were supplied with electricity from the car battery and from the existing tower  
16 power circuit during the measurements.

17

### 18 **2.2 Setup of the car DOAS zenith-sky measurements**

19 An optical fibre was connected to the spectrometer and threaded through an aluminium bracket to  
20 the outside of the car, where it was fixed to a small aluminium plate by duct tape. In order to prevent  
21 direct sunlight from entering the optical fibre, a cylindrical plastic tube was used for shading the  
22 entrance. The field of view of the optical fibre was characterized in the laboratory to be about  $\pm 5^\circ$ .  
23 As the telescope was directed to the zenith, no large errors are expected for the retrieval of  
24 tropospheric vertical NO<sub>2</sub> columns in this case as light path length is relatively insensitive to small  
25 deviations of the pointing from the zenith direction. For stability reasons, the bracket was clamped  
26 by the two door windows of the rear area. The geographical position of the car was recorded by a  
27 GPS receiver, which was connected to and powered by a USB port of the laptop computer.



1 The overall approach was to keep the measurement system simple. Therefore, only the zenith-  
2 direction was implemented which is insensitive to changes in pointing as from telescope  
3 misalignments or car movements. Pointing the instrument closer to the horizon increases the  
4 sensitivity to tropospheric NO<sub>2</sub>, but introduces additional complication as pointing accuracy in a  
5 moving car becomes an issue. Experience also showed that in a city environment, a large fraction  
6 of the measurements at 22° or 30° elevation, for example, is affected by blocking from houses,  
7 trees or other vehicles. As shown in previous studies (e.g. Wagner et al., 2010; Shaiganfar et al.,  
8 2011), the air mass factor for measurements at 22° and 30° depends on the relative azimuth between  
9 the telescope orientation and the sun, necessitating computation of the car heading from GPS data  
10 which can be complex in typical city traffic situations. In summary, the choice was made to use a  
11 simple and robust method at the expense of reduced sensitivity.

12 A total of twenty identical car circuits around Vienna were performed on nine days in April,  
13 September, October, and November 2015 within the metropolitan area of Vienna (see Table 2).  
14 Each drive spanned about 110 km and lasted about 1.5 hours. In order to minimize the effect of  
15 clouds and wind speed, measurements were performed in the morning rather than in the afternoon.  
16 After a successful test phase of the car DOAS zenith-sky measurements on 10 April 2015, more  
17 days were planned in fall of the same year, including working days and days on weekends as well  
18 as days with different wind conditions. Measurements between April and September, e.g. during  
19 the summer season, were unfortunately not possible due to other priorities and due the fact that the  
20 authors were not located in Vienna during that time.

21 Figure 1 illustrates an exemplary overview of a single car journey performed on 10 April 2015  
22 between 5:27 and 6:59 UT. The starting point of each drive was within the Municipality of  
23 Wolkersdorf im Weinviertel (48° 22' 59'' N, 16° 31' 05'' E), a small city located in Lower Austria,  
24 about 10 km north of Vienna and away from large sources of NO<sub>x</sub>. From there, the journey was  
25 planned to cover one of the busiest motorways in Austria, pass by known emission sources (e.g.  
26 power plants), and drive round one of the largest inland refineries in Europe, before heading back  
27 to the starting point on a different route.

28

### 29 **2.3 Setup of tower DOAS off-axis measurements**



1 The same DOAS instrument was used for the measurements performed from the Café at the Vienna  
2 Danube Tower (48° 14' 25" N, 16° 24' 36" E), which is rotating at about 160 m above ground  
3 (www.donauturm.at). Due to its geographical location (about 4.5 km to the northeast of the city  
4 center), it is possible to scan both urban and rural areas during a single anti-clockwise 360° rotation  
5 (duration = 26.5 minutes). In contrast to the car DOAS zenith-sky measurements (see Sect. 2.2),  
6 the telescope was directed towards the horizon at an elevation angle of 0°. An optical lens was  
7 placed in front of the light fibre entrance to reduce the field of view of the instrument to about 0.8°.  
8 Both the lens and the entrance of the optical fibre were protected from direct sunlight by a purpose-  
9 built cardboard. Because the scattered sunlight was passing through a thick glass window, no UV  
10 spectra could be recorded by the DOAS instrument from the rotating tower platform.

11 Tower DOAS off-axis observations were performed on five days in April and May 2016. More  
12 than thirty 360° scans of Vienna were recorded, each of them for an individual rotations of the  
13 Café. For reasons of simplicity and accessibility, zenith-sky measurements were only taken  
14 afterwards from the open terrace, which is located a few meters below.

15 As the Vienna Danube Tower does not provide information on the exact orientation of the platform,  
16 and due to the fact that the signal of the GPS receiver was not accurate enough to reliably determine  
17 the position along the circle, the horizontal viewing angle was determined by the following  
18 approach: The DC Tower 1, the tallest skyscraper in Austria, which is located in about 1 km  
19 distance from the Vienna Danube Tower, comes into field of view once every rotation and  
20 considerably reduces the signal (see Fig. 2). According to Google Earth, the position of the Vienna  
21 Danube Tower relative to this skyscraper is 167° (nearly south). By assuming that the rotation  
22 speed and the alignment on intensity minima are constant, the horizontal viewing angle can be  
23 determined from the periodic sharp reduction in intensity.

24

### 25 **3 Data analysis**

#### 26 **3.1 DOAS analysis**

27 The spectral measurements as obtained during the individual car journeys and tower platform  
28 rotations are analyzed using the DOAS technique applying a nonlinear least-squares fitting





1 algorithm. The spectral retrieval of NO<sub>2</sub> differential slant column densities (DSCDs) is based on a  
2 fitting window between 425 and 490 nm, a polynomial degree of five (car DOAS zenith-sky) and  
3 seven (tower DOAS off-axis), and a wavelength calibration using data from the Solar atlas of  
4 Kurucz et al., (1984). These general settings have been commonly used in recent studies for the  
5 retrieval of NO<sub>2</sub> DSCDs from ground-based DOAS-type measurements (e.g. Roscoe et al., 2010).  
6 High resolution absorption cross-sections of O<sub>3</sub>, NO<sub>2</sub>, O<sub>4</sub>, H<sub>2</sub>O, and a pseudo-cross section  
7 accounting for rotational Raman scattering as computed with QDOAS (Danckert et al., 2015) have  
8 been included in the two retrieval settings (see Table 1). The motivation for using a higher  
9 polynomial degree in the analysis of the horizon measurements are large broadband residuals found  
10 in the data. These residuals are attributed to the fact that the horizon measurements were taken  
11 through thick multi-layer glass while the zenith-sky measurement was taken outdoors.

12 Exemplary car DOAS zenith-sky fit results, recorded on 10 April 2015 (SZA = 47.68°) under  
13 elevated NO<sub>2</sub> pollution (DSCD = 4.02 × 10<sup>16</sup> molec cm<sup>-2</sup>), are shown in Fig. 3 (left panels). In some  
14 parts of the route, the zenith view of the instrument is obstructed by tunnels, bridges or other  
15 objects. These measurements were identified using an intensity criterion and removed from the  
16 data set. However, some outliers having unrealistically high values of NO<sub>2</sub> are still present in the  
17 data set, which strongly correlate with exceptional high chi-square values. Consequently, we only  
18 consider NO<sub>2</sub> DSCDs with chi-square values < 2.5 × 10<sup>-3</sup> for further analysis. Noontime  
19 measurements of three selected days, taken in rural areas and close to air quality monitoring stations  
20 are used as reference measurements (see Sect. 3.2.3 and Table 2).

21 Exemplary tower DOAS off-axis fit results obtained from a spectra recorded on 29 April 2016  
22 (SZA = 66.99°) under elevated NO<sub>2</sub> pollution (DSCD = 1.46 × 10<sup>17</sup> molec cm<sup>-2</sup>) are shown in Fig.  
23 3 (right panels). When comparing the two fit results, it becomes clear that the absorption by NO<sub>2</sub>  
24 in the horizontal path is larger by a factor of 3.6 in this case. This is because most of the NO<sub>2</sub> in  
25 urban environments is found in the boundary layer, close to the ground.

26

## 27 **3.2 Car DOAS measurements of tropospheric NO<sub>2</sub>**

### 28 **3.2.1 Temporal resolution and computation of horizontal NO<sub>2</sub> gradients**



1 In order to obtain some information about the signal to noise ratio of the instrument and the  
2 horizontal gradients of NO<sub>2</sub> present in the city, the temporal resolution of the car DOAS zenith-  
3 sky measurements was initially set to 0.5 seconds. The collected spectra were then averaged over  
4 intervals of 5 seconds (see Fig. 4), which corresponds to a traveled distance of about 100 m. An  
5 averaging interval of 5 seconds was also used by Constantin et al. (2013) for their mobile  
6 measurements.

7 The upper panel in Fig. 4 shows the temporal evolution of NO<sub>2</sub> DSCDs on 3 November 2015. The  
8 red and blue lines represent the full resolution of 0.5 seconds and averaged values, respectively.  
9 While the full resolution is noisy (maximum deviation  $\sim 5 \times 10^{15}$  molec cm<sup>-2</sup>), the averaged values  
10 follow the general pattern of NO<sub>2</sub> along the car drives. For better clarity, the middle panel illustrates  
11 a shorter section of that day, indicated by the green lines in the upper panel. The same is true for  
12 the lower panel, which represents a short section of the middle panel. Based on these results we  
13 argue that the selection of 5 seconds as an averaging interval appears to be optimal and a good  
14 compromise in our study, in spite of more information being found in the high-frequency data in  
15 some cases.

16 In addition to mapping the spatial distribution of NO<sub>2</sub> in Vienna, it is also interesting to evaluate  
17 typical horizontal gradients within the city. The identification of such mean horizontal gradients of  
18 NO<sub>2</sub> along the individual car routes is based on the following approach. Firstly, horizontal distances  
19 between start and end point of individual car DOAS zenith-sky measurements at the full resolution  
20 of 0.5 seconds are calculated and summed. Secondly, NO<sub>2</sub> DSCDs at the same time resolution are  
21 interpolated on 100 m bins as obtained from the first calculation step. Thirdly, absolute differences  
22 of NO<sub>2</sub> DSCDs are derived for each pair of consecutive interpolated values within 5 km. In a final  
23 step, absolute differences are averaged along the car track in order to compute a mean horizontal  
24 gradient for each single car lap.

25

### 26 **3.2.2 Stratospheric NO<sub>2</sub> columns**

27 The stratospheric correction in our study is based on stratospheric NO<sub>2</sub> fields as simulated by the  
28 Bremen 3d CTM (B3dCTM) and scaled to satellite observations from the Global Monitoring



1 Instrument 2 (GOME-2) over a selected region in the Pacific (180°-140° W, 48°-48.5° N). This  
2 scaling is necessary as there is an offset between modeled and measured NO<sub>2</sub> amounts.

3 Briefly, the B3dCTM, which evolved from SLIMCAT (Chipperfield, 1999), is a combined model  
4 approach based on the “Bremen transport model” (Sinnhuber et al., 2003a) and the chemistry code  
5 of the “Bremen two-dimensional model of the stratosphere and mesosphere” (Sinnhuber et al.,  
6 2003b; Winkler et al., 2008). It is driven by ECMWF ERA Interim meteorological reanalysis fields  
7 (Dee et al., 2011).

8 Exemplary simulated stratospheric NO<sub>2</sub> columns above Vienna as obtained from B3dCTM are  
9 shown in Fig. 5 for 19 October 2015. While stratospheric NO<sub>2</sub> amounts sharply decrease in the  
10 morning due to photolysis of NO<sub>2</sub>, the observed increase of NO<sub>2</sub> over the day is the result of  
11 dinitrogen pentoxide (N<sub>2</sub>O<sub>5</sub>) photolysis. The green rectangle indicates the start (06:57 UT) and end  
12 time (09:56 UT) of car DOAS zenith-sky measurements performed on 19 October 2015 (see also  
13 Table 2).

14

### 15 **3.2.3 Conversion to tropospheric NO<sub>2</sub> vertical column densities**

16 The conversion of NO<sub>2</sub> DSCDs obtained from car DOAS zenith-sky measurements into NO<sub>2</sub>  
17 tropospheric vertical column densities (VCD<sub>tropo</sub>) is based on the approach by Wagner et al. (2010)  
18 and Constantin et al. (2013). The authors of the latter study have used a similar zenith-sky DOAS  
19 system on a car to derive tropospheric NO<sub>2</sub> amounts in Romania. VCD<sub>tropo</sub> from car DOAS zenith-  
20 sky measurements is determined via the following equation:

$$21 \quad VCD_{tropo} = \frac{DSCD_{meas} + SCD_{ref} - VCD_{strato} * AMF_{strato}}{AMF_{tropo}}, \quad (1)$$

22 where DSCD<sub>meas</sub> is obtained from the car DOAS zenith-sky measurements by applying the DOAS  
23 analysis (see Sect. 3.1). SCD<sub>ref</sub> is the slant column in the reference spectrum, which cannot be  
24 measured directly when applying the zenith-sky viewing mode only. Moreover, SCD<sub>ref</sub> has both  
25 stratospheric and tropospheric amounts, which are estimated with different approaches in the  
26 literature. The tropospheric NO<sub>2</sub> signal in SCD<sub>ref</sub> in our study is calculated by applying the  
27 empirical relationship between VCD<sub>tropo</sub> and in situ NO<sub>2</sub> mixing ratios as reported in Kramer et al.



1 (2008). To be more specific, the estimation of tropospheric NO<sub>2</sub> amounts in SCD<sub>ref</sub> is conducted  
2 for the time and location of the three selected reference measurements taken in rural areas outside  
3 the boundaries of Vienna and about 13 km (10 April 2015) and 3 km (27 September and 23  
4 October) away from the nearest air quality monitoring station. More details on data from air quality  
5 monitoring stations are given in the following Sect. 3.3. VCD<sub>strato</sub> is derived from B3dCTM  
6 simulations and scaled to GOME-2 observations (see Sect. 3.2.2). Stratospheric and tropospheric  
7 airmass factors are calculated with the SCIATRAN radiative transfer model (Rozanov et al., 2014).  
8 For the latter case, the AMF is calculated for a wavelength of 460 nm by assuming that NO<sub>2</sub> is  
9 well-mixed between the ground surface and an altitude of 1 km. The computed stratospheric and  
10 tropospheric AMFs as a function of SZA are shown in the left and right panels of Fig. 6,  
11 respectively.

12

### 13 3.3 In situ measurements of NO<sub>2</sub>

14 For the estimation of tropospheric NO<sub>2</sub> amounts in SCD<sub>ref</sub> as well as for the comparison of NO<sub>2</sub>  
15 VCD<sub>tropo</sub> obtained from car DOAS zenith-sky measurements with in situ NO<sub>2</sub> concentrations, data  
16 from more than a dozen air quality monitoring stations in and around Vienna, provided by the  
17 Environment Agency Austria, UBA (Umweltbundesamt), are used.

18 Tropospheric NO<sub>2</sub> amounts in SCD<sub>ref</sub> are calculated by converting simultaneous in situ NO<sub>2</sub>  
19 measurements from the air quality monitoring stations in Gänserndorf (10 April 2015) and  
20 Wolkersdorf (27 September and 23 October 2015) into VCD<sub>tropo</sub> applying the empirical  
21 relationship between concurrent MAX-DOAS and urban background in situ measurements  
22 (Kramer et al., 2008):

$$23 \quad y = 0.036x + 0.018, \quad (2)$$

24 where  $y$  is the tropospheric NO<sub>2</sub> VCD (tropospheric NO<sub>2</sub> amount in SCD<sub>ref</sub> in our study) in units  
25 of 10<sup>16</sup> molec cm<sup>-2</sup> and  $x$  denotes the in situ NO<sub>2</sub> mixing ratios in units ppb. The conversion of in  
26 situ NO<sub>2</sub> concentrations into in situ mixing ratios in our study is described in Sect. 3.5.



1 The tropospheric background values in  $SCD_{ref}$  as determined with Eq. 2 are estimated at  $1.3 \times 10^{15}$ ,  
2  $1.1 \times 10^{15}$ , and  $2.2 \times 10^{15}$  molecules  $cm^{-2}$  on 10 April, 27 September, and 23 October, respectively.  
3 We note that the extrapolation of the empirical relationship to our measurements is critical in a  
4 sense that meteorological conditions and emissions are not the same in Leicester and Vienna. Due  
5 to the fact that  $SCD_{ref}$  measurements were taken outside of Vienna in our study, with in situ  
6 measurements of  $NO_2$  being in the range of 2.5 to 6 ppb on those three days and indicating rather  
7 low tropospheric  $NO_2$  amounts, the error is assumed to be likewise low in this case.

8 For the comparison of car DOAS zenith-sky and in situ  $NO_2$  observations, we have selected half-  
9 hour averages of  $NO_2$  concentrations from seven stations in Lower Austria and eight stations in  
10 Vienna that are within 5 km from the car route (see Table 3). For both cases, half-hour averages of  
11  $NO_2$  concentrations are converted into mixing ratios (see Sect. 3.5).

12

### 13 **3.4 Mixing-height from ceilometer observations**

14 The conversion of  $VCD_{tropo}$  into mixing ratios as described in the following Sect. 3.5 requires,  
15 besides meteorological measurements of pressure and temperature, information on the planetary  
16 boundary layer depth (also known as mixing-height). The Austrian official weather service, ZAMG  
17 (Zentralanstalt für Meteorologie und Geodynamik), performs operational aerosol-layer height  
18 measurements with a Vaisala CL51 ceilometer at the Hohe Warte site in the North West of Vienna  
19 ( $48^\circ 14' 55''$  N,  $16^\circ 21' 23''$  E). Mixing-height (MH) time series are obtained from these  
20 measurements by removing unrealistic nocturnal aerosol-layer height values, avoiding outliers,  
21 filling data gaps by linear interpolation, and smoothing (Lotteraner and Piringer, 2016). Mixing-  
22 height data at a temporal resolution of 5 minutes were provided by ZAMG for those days when car  
23 DOAS zenith-sky measurements were carried out.

24

### 25 **3.5 Comparison of $NO_2$ mixing ratios obtained from car DOAS zenith-sky and in situ** 26 **measurements**



1 The comparison between the two independent NO<sub>2</sub> observations (car DOAS zenith-sky versus in  
2 situ) is based on gridding the data of both measurement techniques onto a 0.01° x 0.01° spatial  
3 resolution. For a better comparison, NO<sub>2</sub> VCD<sub>tropo</sub> as obtained from car DOAS zenith-sky  
4 measurements as well as in situ NO<sub>2</sub> concentrations are converted into mixing ratios. The former  
5 conversion is based on recommendations made in Knepp et al. (2013). The authors of that study  
6 have converted Pandora tropospheric NO<sub>2</sub> values into mixing ratio values by applying a planetary  
7 boundary layer (PBL) height correction factor. Although this approach assumes a constant mixing  
8 ratio in the PBL, which is not necessarily correct in an urban environment, it accounts for the  
9 variability in MH throughout the day. We follow their approach and estimate boundary layer  
10 mixing ratios of NO<sub>2</sub> ( $X_{NO_2}$ ) via the following equation:

$$11 \quad \text{Car DOAS (BL)} X_{NO_2} = \frac{VCD_{tropo}}{MH \cdot n_a}, \quad (3)$$

12 where MH is the mixing-height (PBL in their study) and  $n_a$  denotes the number density of air (N  
13 in their study). Here, we use lap averages for MH as calculated from the data in 5 minute resolution  
14 provided by ZAMG (see Sect. 3.4). The standard deviation of these lap averages generally ranges  
15 between 10 and 50 m but can be as high as 200 m when wind speeds are high (see Table 2). The  
16 number density of air, which is related to the atmospheric pressure by the ideal gas law, is also  
17 averaged over the individual car laps. Meteorological measurements of pressure (p) and  
18 temperature (T) used for the calculation of  $n_a$  are provided by the BOKU (Universität für  
19 Bodenkultur) weather station, located in the North West of Vienna (48° 14' 16.45" N, 16° 19' 54"  
20 E). We note that the weather station is located about 100 m higher than the altitude level of the car  
21 route. Thus, pressure might be slightly lower when compared to the pressure level 100 m below.  
22 On the other hand, the weather station is also located outside of the city center, at the foot of the  
23 hills in the Northwest and in a less densely populated residential area with many green areas,  
24 resulting in slightly cooler temperatures than expected for other places along the car route.  
25 Following this reasoning, it becomes clear that the altitude difference might cancel in the  
26 calculation of  $n_a$  (see Eq. 3) and also in the following Eq. 5.

27 Recently, Dieudonne et al. (2013) highlighted the fact that large vertical gradients of NO<sub>2</sub>  
28 concentrations exist over urban areas. The authors of that study suggest that the averaged  
29 concentration within the PBL is only about 25% of NO<sub>2</sub> surface concentration measurements when



1 NO<sub>2</sub> profiles from chemistry-transport models are assumed for the PBL. Following this reasoning,  
2 Car DOAS (BL) X<sub>NO<sub>2</sub></sub> as estimated via Eq. 3 does not represent NO<sub>2</sub> near-surface mixing ratios  
3 sufficiently well and a comparison with NO<sub>2</sub> as obtained from air quality monitoring stations and  
4 converted into In situ X<sub>NO<sub>2</sub></sub> (see Eq. 5) is not yet reasonable. Consequently, an empirical approach  
5 for estimating near-surface NO<sub>2</sub> mixing ratios from the car DOAS zenith-sky measurements was  
6 developed, in addition to Car DOAS (BL) X<sub>NO<sub>2</sub></sub>.

7 In order to achieve optimal agreement between car DOAS zenith-sky measurements and in situ  
8 observations in our study, we include four parameters that are expected to affect the vertical NO<sub>2</sub>  
9 gradients and conduct a linear regression analysis as follows:

$$10 \quad Y = \beta_0 + \beta_1 X_1 + \beta_2 X_2 + \beta_3 X_3 + \beta_4 X_4 + \varepsilon, \quad (4)$$

11 where  $Y$  is the expected value of the dependent variable In situ X<sub>NO<sub>2</sub></sub> and  $X_1$ ,  $X_2$ ,  $X_3$ , and  $X_4$  are the  
12 independent variables VCD<sub>tropo</sub> NO<sub>2</sub>, MH, wind speed, and  $n_a$ , respectively (see Table 2).

13 The conversion of in situ NO<sub>2</sub> concentrations ( $c_m$ ) into mixing ratios is based on the equation:

$$14 \quad \text{In situ } X_{NO_2} = c_m \frac{1}{M_i} * \frac{RT}{p}, \quad (5)$$

15 where  $M_i$  is the molecular weight of NO<sub>2</sub> and  $R$  denotes the universal gas constant. As for the  
16 calculation of  $n_a$ ,  $p$  and  $T$  measurements at a 10 minute resolution are taken from the BOKU  
17 weather station and averaged for the individual car laps.

18 All NO<sub>2</sub> mixing ratio values within individual grid cells are averaged and then compared with each  
19 other.

20

### 21 **3.6 Meteorological measurements of wind direction and wind speed**

22 Most of the emission sources other than traffic are located in the South-East of Vienna. The wind  
23 blew exactly from this direction on several days when car DOAS zenith-sky measurements were  
24 carried out. In addition, the car journey was planned to include the motorway along the Danube  
25 River, spanning a distance of about 20 km from North-West (48° 21' 25'' N, 16° 18' 25'' E) to



1 South-East ( $48^{\circ} 12' 32''$  N,  $16^{\circ} 26' 24''$  E). These are prerequisites for the optimal analysis of the  
2 evolution of  $\text{NO}_2$  in space and time, in particular on days where wind was blowing either from  
3 North-West (NW) or South-East (SE). As there are no large sources of  $\text{NO}_x$  located in the NW, we  
4 rather focus on days when wind was blowing from the SE.

5 Data on wind direction and wind speed are provided by ZAMG. We have selected such data from  
6 four stations in Lower Austria and five stations in Vienna that are in close proximity to the car  
7 route (see Table 4). The temporal resolution of these measurements is 10 minutes. Instead of  
8 attempting to map the wind direction to the car route in time, we have averaged these measurements  
9 over the period between start and end time of each car journey and calculated the standard deviation  
10 (see Table 2).

11

## 12 **3.7 Tower DOAS measurements of tropospheric $\text{NO}_2$**

### 13 **3.7.1 Temporal resolution and normalization of $\text{NO}_2$ DSCDs with $\text{O}_4$**

14 Compared to the car DOAS zenith-sky measurements, the temporal resolution of spectral  
15 measurements performed on the rotating tower platform is higher (0.025 s). This is because of the  
16 relatively fast rotation speed resulting in a full  $360^{\circ}$  rotation within only 26.5 minutes. Again, these  
17 temporally high-resolved spectral measurements are averaged over 10 seconds. After the averaging  
18 procedure, roughly 150 measurements remain for a single  $360^{\circ}$  rotation. These observations are  
19 then interpolated on  $3.6^{\circ}$  segments, resulting in 100 measurements for one single rotation.

20 One of the main drawbacks of the measurements is that only one reference measurement was taken  
21 after the measurements. This was because no zenith-sky measurement was possible from within  
22 the restaurant, and no second DOAS system was available during that time for parallel  
23 measurements from the surface. Therefore, a fixed zenith spectrum has to be used instead of a  
24 sequential one, resulting in an increasing effect of a changing tropospheric light path (e.g. due to  
25 geometry, aerosols, phase function etc.) with increasing time difference between the off-axis and  
26 fixed zenith spectra. One way of overcoming this problem is to normalize  $\text{NO}_2$  DSCDs with  $\text{O}_4$   
27 DSCDs, which is done for all measurements taken.





1

## 2 **3.7.2 Computation of path-averaged NO<sub>2</sub> mixing ratios**

3 A modified geometrical approach (MGA) for estimating long-path averaged mixing ratios of trace  
4 gases (e.g. NO<sub>2</sub>) from MAX-DOAS measurements at high-altitude sites was proposed in a recent  
5 study by Gomez et al. (2014). The method assumes a single-scattering geometry and a scattering  
6 point altitude close to that of the instrument. Under these assumptions, the slant paths of the  
7 zenith ( $\alpha = 90^\circ$ ) and horizontal ( $\alpha = 0^\circ$ ) measurements are identical up to the scattering point  
8 and thus, cancel in the DSCD when using a zenith-sky background spectrum close in time. For  
9 measurements performed at higher altitudes, the MGA can be applied without any correction  
10 factors, in particular when the instrument is located well above the PBL and aerosol amounts are  
11 negligibly low (Schreier et al., 2016). For MAX-DOAS measurements carried out close to the  
12 ground level, however, the MGA is limited because of a substantial aerosol load and correction  
13 factors are needed (Sinnreich et al., 2013). Nevertheless, Seyler et al. (2017) have recently  
14 successfully utilized the MGA for MAX-DOAS measurements of shipping emissions in the  
15 German Bight – without the use of correction factors. According to their findings, typical lengths  
16 of horizontal light paths in the visible spectral range are in the range of  $12.9 \pm 4.5$  km on average  
17 and can reach up to 15 km on days with optimal visibility. It should be noted, however, that the  
18 non-consideration of correction factors in polluted environments such as the German Bight will  
19 lead to a systematic overestimation of horizontal path lengths, depending on the aerosol load.

20 In our study, where the rotating tower platform is also located close to the ground level, we  
21 overcome this problem by making the following assumptions. Firstly, we assume that the signal  
22 for horizontal measurements ( $\alpha = 0^\circ$ ) is dominated by the horizontal part of the light path after the  
23 last scattering event. Secondly, a hill named Kahlenberg (484 m a.s.l.) and being located in the  
24 Northwest of the Vienna Danube Tower ( $305^\circ$ ) comes into field of view once every rotation. We  
25 assume that the hill limits the horizontal optical path length (hOPL) under clear sky conditions and  
26 use the distance between the summit of the hill and the Vienna Danube Tower (6.95 km) as  
27 normalization value. The conversion of DSCD O<sub>4</sub> at  $\alpha = 0^\circ$  is realized by relating this distance with  
28 the obtained DSCD O<sub>4</sub> value at  $305^\circ$  and applying the resulting relationship to all other DSCD O<sub>4</sub>  
29 values observed during the same tower platform rotation. We assume that the change of DSCD



1 NO<sub>2</sub> in the vertical ( $\alpha = 90^\circ$ ) can be neglected for (polluted) urban environments over the course  
2 of one tower rotation. The latter assumption has to be made because no sequential zenith-sky  
3 spectra are available. Therefore, path-averaged NO<sub>2</sub> mixing ratios are only estimated and presented  
4 for the last tower rotations of the individual days, having the zenith-sky reference spectrum as close  
5 as possible in time.

6 When taking all these assumptions into consideration, path-averaged mixing ratios of NO<sub>2</sub> can be  
7 estimated with the following equation:

$$8 \quad \text{Tower DOAS } X_{NO_2} = \left( \frac{DSCD NO_2}{hOPL} \right) / n_a \quad (6)$$

9 For the calculation of  $n_a$ , rotation averages of pressure and temperature as provided by the BOKU  
10 weather station are used (see Sect. 3.5).

11

## 12 **4 Results and discussion**

### 13 **4.1 Horizontal gradients of NO<sub>2</sub> DSCDs**

14 As the car DOAS zenith-sky measurements provide in addition to the temporal distribution the  
15 horizontal variation of NO<sub>2</sub>, the method described in Sect. 3.2.1 is applied to the car DOAS zenith-  
16 sky observations to determine horizontal gradients of NO<sub>2</sub>.

17 In Figure 7, typical examples of such horizontal gradients are presented for 27 September, 6  
18 October and 3 November 2015 – three days with different wind conditions, temperature levels and  
19 tropospheric NO<sub>2</sub> amounts (see Table 2). In general, an increase in absolute NO<sub>2</sub> differences with  
20 increasing distance from the individual starting points is found. While absolute NO<sub>2</sub> differences  
21 sharply increase within the first one or two kilometers for most of the journeys, the increase  
22 significantly weakens during the remaining kilometers. During the first kilometer, absolute NO<sub>2</sub>  
23 differences increase by a factor of 1.5 to 4, depending on the overall NO<sub>2</sub> level on the investigated  
24 days. While the absolute NO<sub>2</sub> differences rise by a factor of about two within the first two  
25 kilometers on 27 September, an increase by a factor of almost four is found for the same distance  
26 on the more polluted 6 October 2015.



1 The results imply that the magnitude of absolute NO<sub>2</sub> differences is linked to the magnitude of  
2 tropospheric NO<sub>2</sub> amounts observed. On the other hand, it is difficult to detect the factors affecting  
3 the shape of the derived curves. Interestingly, we found only small differences in the shape and  
4 magnitude of horizontal NO<sub>2</sub> gradients when comparing individual car journeys of single days with  
5 each other. Only for days with significant changes in wind direction (e.g. 27 September 2015) are  
6 the differences in magnitude obvious, when the single laps are compared with each other. While  
7 the curves of 10 April (not shown) and 6 October are similar in shape, the typical sharp increase  
8 within the first two kilometers is not observed for 3 November, although average values of wind  
9 speed, wind direction and mixing-height were similar on those days (see Table 2). It is not clear  
10 why the shape of NO<sub>2</sub> as a function of distance observed on 3 November differs from those found  
11 on the other two days. One reason could be variations in photochemistry and/or emissions and/or  
12 dilution of NO<sub>x</sub>. It is interesting to note that 3 November 2015 was clearly the coldest day with  
13 temperatures below 5°C (see Table 2). As a result, we argue that the characteristic horizontal NO<sub>2</sub>  
14 scale of the observed NO<sub>2</sub> fields in Vienna is on the order of 1 to 2 km.

15

#### 16 **4.2 Temporal evolution of tropospheric NO<sub>2</sub>**

17 Figure 8 shows typical car DOAS zenith-sky measurements of NO<sub>2</sub> performed on 10 April 2015.  
18 The black and red curves represent DSCD<sub>meas</sub> and VCD<sub>tropo</sub>, respectively. The stratospheric NO<sub>2</sub>  
19 amounts as simulated by B3dCTM and scaled to GOME-2 observations (see Sect. 3.2.3) are  
20 illustrated by the blue line. Clearly, stratospheric NO<sub>2</sub> is relatively low in this case of increased  
21 tropospheric NO<sub>2</sub> levels when compared to VCD<sub>tropo</sub>. The relatively small diurnal increase of NO<sub>2</sub>  
22 in the stratosphere can hardly be seen for the 6-hour period. There are individual peaks in NO<sub>2</sub>  
23 throughout the morning of 10 April 2015. While the longer lasting NO<sub>2</sub> peaks are probably  
24 connected to pollution from traffic, sharp peaks rather indicate some outflow of NO<sub>2</sub> from the  
25 refinery and/or other local static emission sources. The magnitude of observed NO<sub>2</sub> VCD<sub>tropo</sub> is in  
26 good agreement with measurements performed around the German cities Mannheim and  
27 Ludwigshafen as well as in the Romanian city Braila (Ibrahim et al., 2010; Dragomir et al., 2015).  
28 As expected, significantly higher values of NO<sub>2</sub> VCD<sub>tropo</sub> were observed by Wang et al. (2012) in  
29 the central urban area of Shanghai, China.



1 In the following, the small-scale transport of NO<sub>2</sub> is evaluated along the Donauufer motorway  
2 (A22) in more detail. The A22 motorway, which is identifiable in Fig. 1 by azure blue and turquoise  
3 dots (NW to SE), is one of the busiest roads in Vienna, in particular in the south-eastern area, where  
4 many commuters take the Südosttangente motorway (A23) at the motorway junction  
5 Kaisermühlen. The A23 is another busy road in Austria having about 160000 passenger cars  
6 driving every day on average ([www.vcoe.at](http://www.vcoe.at)). As a consequence, NO<sub>2</sub> levels are expected to be  
7 significantly increased in this area, in particular during the morning and evening rush hours.

8 The NO<sub>2</sub> variation along the A22 motorway is shown in Fig. 9 for Friday, 10 April and Friday, 3  
9 November 2015 as a function of cumulative distance, where the starting and end points are in the  
10 NW and SE of the A22 motorway. The red, blue, and green curves represent NO<sub>2</sub> VCD<sub>tropo</sub> during  
11 the first, second, and third drive, respectively. In order to not confuse the reader, the first and second  
12 rounds of days with measurements taken only during two rounds are here referred to as round two  
13 and three, starting approximately at 07:00 and 08:30 UT, respectively (see Table 2). While wind  
14 was blowing from SE on both days, averages of wind speed were slightly higher on 3 November.

15 On 10 April, highest NO<sub>2</sub> VCD<sub>tropo</sub> is observed in the SE rather than in the NW during the first  
16 drive. This seems reasonable as the traffic volume is generally largest in this area, in particular  
17 during the morning rush-hour, which is captured by the first drive of that day. NO<sub>2</sub> loads are then  
18 moving to the NW of the A22 motorway, because air masses are transported from SE. A clear shift  
19 of NO<sub>2</sub> pollution from SE to NW is observed on 10 April 2015. Highest NO<sub>2</sub> VCD<sub>tropo</sub> during the  
20 first ( $\sim 2.3 \times 10^{16}$  molec cm<sup>-2</sup>), second ( $< 2.5 \times 10^{16}$  molec cm<sup>-2</sup>), and third drive ( $> 2.5 \times 10^{16}$  molec  
21 cm<sup>-2</sup>) are located around 19.5, 18.5, and 8.5 km away from the starting point in the NW,  
22 respectively. Interestingly, the observed NO<sub>2</sub> peak during the last drive is very pronounced. We  
23 attribute this to the NO<sub>2</sub> formation via the chemical reaction of NO with ozone towards noon time.  
24 The topography in this area could also be responsible for these high NO<sub>2</sub> levels. There are two hills  
25 left (Bisamberg, 358 m a.s.l.) and right (Kahlenberg, 484 m a.s.l.) of the Danube River. As a  
26 consequence, the pollution load could be channeled between the two hills, leading to a localized  
27 increase in NO<sub>2</sub> amounts in this area.

28 The distance of NO<sub>2</sub> transport appears larger between the second and third drives when compared  
29 with distances of NO<sub>2</sub> transport between the first and second journey. This might be related to the



1 increase in average wind speed throughout the morning (see Table 2). Overall, the distance of NO<sub>2</sub>  
2 transport on 10 April 2015 is in good agreement with average wind speed. Due to higher wind  
3 speeds on 3 November 2015, the expected peaks of NO<sub>2</sub> in the NW during the third journey cannot  
4 be seen anymore. This might be related to the high averaged wind speeds during the second and  
5 third drives (between 8 and 10 km h<sup>-1</sup>) and thus, a distance of transport exceeding the area of  
6 evaluation. On the other hand, a clear shift of elevated NO<sub>2</sub> amounts into the NW is also observed  
7 for the second round on 3 November 2015. It is interesting to note that the horizontal extent of  
8 elevated NO<sub>2</sub> amounts during the third round of 10 April and during the second round of 3  
9 November 2015 spans about 8 km in both cases – under similar wind speeds. We argue that this is  
10 a characteristic horizontal extent of a NO<sub>2</sub> plume resulting from morning rush-hour traffic in  
11 Vienna under calm southeasterly winds.

12 The spatial and temporal variation in tropospheric NO<sub>2</sub> amounts is also evaluated by analyzing the  
13 tower DOAS off-axis measurements. In order to correct light path lengths in the troposphere, NO<sub>2</sub>  
14 DSCDs are normalized with O<sub>4</sub> DSCDs. When looking at the time series of intensity (see Fig. 2),  
15 NO<sub>2</sub>, and O<sub>4</sub> (Fig. 10), it becomes apparent that these parameters show variations as a function of  
16 azimuth angle. This variation is repeated with each further tower platform rotation. Although some  
17 similarity is found between DSCD NO<sub>2</sub> and O<sub>4</sub>, the highest and lowest amounts of both trace gases  
18 are somehow shifted on the x-axis. Some similarity between DSCD O<sub>4</sub> and NO<sub>2</sub>, which is observed  
19 on all five days (not shown), is attributed to changes in the light path. Interestingly, the  
20 normalization with O<sub>4</sub> slightly changes the azimuthal position of the pollution peaks towards the  
21 city center.

22 The geographical distribution of DSCD NO<sub>2</sub>/O<sub>4</sub> is shown in Fig. 11 for 10 May 2016, when tower  
23 DOAS off-axis measurements during nine platform rotations were collected. The values plotted on  
24 the map are mean NO<sub>2</sub>/O<sub>4</sub> values and the radius is the O<sub>4</sub> column. On that day, wind was mainly  
25 blowing from easterly to southeasterly directions. As a result, highest NO<sub>2</sub>/O<sub>4</sub> ratios are observed  
26 towards the city center.

27 The spatial and temporal variability of DSCD NO<sub>2</sub>/O<sub>4</sub> as obtained from tower DOAS off-axis  
28 measurements is shown in Fig. 12 for 9 and 10 May 2016. As already identified from the analysis  
29 of the car DOAS zenith-sky measurements, highest tropospheric NO<sub>2</sub> over Vienna is found in the



1 early morning – a consequence of both a lower (nocturnal) mixing-height and emissions of  $\text{NO}_x$   
2 from morning rush hour traffic. Highest  $\text{NO}_2$  amounts on both days are generally observed over  
3 the city center of Vienna, which is located to the Southwest of the Vienna Danube Tower. A closer  
4 look suggests that DSCD  $\text{NO}_2/\text{O}_4$  is about a factor two larger on 9 May than on the 10 May. While  
5 wind was constantly blowing from the SE on both days, the explanation for this is most likely the  
6 higher wind speeds on 10 May.

7

#### 8 **4.3 Comparison of $\text{NO}_2$ from car DOAS zenith-sky measurements with in situ $\text{NO}_2$**

9 The spatial and temporal evolution of  $\text{NO}_2$  on 10 April 2015 in Vienna as observed by car DOAS  
10 zenith-sky (dots) and in situ measurements (squares) is shown in Fig. 13. Wind direction and wind  
11 speed obtained from local weather stations are indicated by white arrows. The geographical maps  
12 illustrate the spatial distribution of tropospheric  $\text{NO}_2$  during the three performed journeys on that  
13 day. As already highlighted in Sect. 4.2, a clear change in the amount of  $\text{NO}_2$  throughout the  
14 morning is observed along the motorway A22. A large proportion of observed  $\text{NO}_2$  amounts is  
15 produced from traffic emissions of  $\text{NO}_x$  during the morning rush-hour traffic, in particular in the  
16 area southeast of the city center. During the time period of about 4.5 hours between starting and  
17 end point of the measurements performed on that day,  $\text{NO}_2$  is transported over a distance between  
18 10 and 15 km. Another hotspot of increased  $\text{NO}_2$  levels is observed close to an oil refinery in the  
19 SE. The outflow of the refinery is in good agreement with wind direction on that day. As already  
20 mentioned in Sect. 4.2, such peaks of  $\text{NO}_2$  amounts as a result of local static emission sources are  
21 sharper than those originating from typical rush-hour traffic. There is a clear decrease of  
22 tropospheric  $\text{NO}_2$  throughout the morning (see also Table 2), most likely as a consequence of  
23 dilution and/or the reaction of  $\text{NO}_2$  with the hydroxyl radical (OH), which is the largest  $\text{NO}_x$  sink  
24 during daytime.

25 Overall, averages of tropospheric  $\text{NO}_2$  observations were highest on 10 April 2015 and 3 November  
26 2015. We attribute this behavior to the comparatively low wind speeds, and consequent low  
27 dilution.



1 As outlined in Sect. 3.5, the correlation of the two data sets (car DOAS zenith-sky versus in situ)  
2 uses data converted into NO<sub>2</sub> mixing ratios, which are gridded values onto 0.01° x 0.01° cells. The  
3 correlation is performed for each single day where car DOAS zenith-sky measurements were  
4 carried out. The scatter plots including statistics about slope, intercept and correlation coefficient  
5 are illustrated in Fig. 14. Each of the diamonds represents a grid box average of X<sub>NO<sub>2</sub></sub> from car  
6 DOAS zenith-sky measurements as a function of averaged X<sub>NO<sub>2</sub></sub> concentrations from in situ  
7 monitors. The correlation coefficient on 10 April 2015, for example, is 0.8, suggesting a close  
8 linear relationship of the two independent NO<sub>2</sub> measurements on that day (see also Table 2). The  
9 negative offset apparent implies that in situ X<sub>NO<sub>2</sub></sub> is higher than X<sub>NO<sub>2</sub></sub> estimated via Eq. 3. While  
10 this is the case for the grid box averages calculated from measurements taken during the second  
11 and third journeys of that day, X<sub>NO<sub>2</sub></sub> from car DOAS zenith-sky observations seem to be  
12 overestimated during the first journey. X<sub>NO<sub>2</sub></sub> values close to the 1:1 line are also observed on 2  
13 October, the second day, when early morning measurements were performed and when wind was  
14 also blowing from Southeast. The reason for the better agreement in the early morning (e.g. during  
15 the first car journey) could be the lower MH and lower wind speed, resulting in a better vertical  
16 mixing within the shallow boundary layer. The increase in both MH and wind speed throughout  
17 the morning might counteract a vertical mixing of NO<sub>2</sub> loads.

18 Another explanation of the rather underestimated mixing ratio values obtained from car DOAS  
19 zenith-sky measurements observed on the other days is a possible overestimation of tropospheric  
20 AMFs, which are used for the conversion of NO<sub>2</sub> DSCDs (see Eq. 1). Wang et al. (2012) have  
21 reported total uncertainties of tropospheric AMFs in the range of 20-30% for SZAs < 40°. With  
22 increasing SZA towards sunrise/sunset the uncertainties further increase. We note that most of our  
23 car DOAS zenith-sky measurements were performed for SZAs larger than 40°.

24 Kramer et al. (2008) performed a comparison between data from a Concurrent MAX-DOAS  
25 (C-MAX-DOAS) instrument and in situ instruments in the city of Leicester, England. They  
26 highlighted the fact that the relative positions of the in situ instruments to the streets affect the  
27 comparison. In contrast to their study, car DOAS zenith-sky measurements were performed along  
28 motorways in our study. Therefore, this effect can be partly ruled out for the comparison presented  
29 in our study. Difficulties rather arise from losing some of the NO<sub>2</sub> signal at the surface levels  
30 because of the zenith-sky geometry applied for our car DOAS measurements.



1 Nevertheless, large correlation coefficients ( $R = 0.72-0.94$ ) are also observed on the other days  
2 with wind coming from the SE (6, 27 October, and 3 November). In contrast, weak correlation  
3 between the two data sets is observed on days when wind was blowing from the NW (27  
4 September, 19 and 23 October). The reason for the weak correlation on those days is not entirely  
5 clear. However, a closer look reveals that the variability of  $\text{NO}_2$  levels between the performed car  
6 journeys on a single day is only low on days with winds from NW (see Table 2). This might be  
7 related to the fact that high traffic volume but also most of the in situ monitoring station used in  
8 this study are located rather in the SE of the city center than in the NW and thus, the peak of rush-  
9 hour traffic does not show up in the measurements of most of the in situ monitoring stations on  
10 those days.

11 As  $X_{\text{NO}_2}$  estimated via Eq. 3 represent averages within the PBL and thus, values are rather  
12 underestimated when compared to the values obtained from air quality monitoring stations (see  
13 Table 2), a linear regression analysis is introduced (see Eq. 4). The motivation behind this approach  
14 is related to the findings of Dieudonne et al. (2013). The authors of that study highlighted the fact  
15 that the vertical distribution of  $\text{NO}_2$  within the PBL over an urban area is not homogenous. They  
16 also suggested considering the effect of wind speed on the vertical gradient. Therefore, we also  
17 include wind speed in the linear regression analysis.

18 The lap averages of Car DOAS (Surface)  $X_{\text{NO}_2}$  are given in Table 2. Overall, the values are in good  
19 agreement with the lap averages obtained from the air quality monitoring stations. For a better  
20 view, the modeled mixing ratios are plotted against mixing ratios obtained from in situ  
21 measurements in Fig. 15. The gray dotted lines represent the  $\pm 25\%$  level, meaning that all the  
22 values estimated via Eq. 4 are within  $\pm 25\%$ , with the exception of values lower than 10 ppb. The  
23 reason for these larger differences could be a reduced signal-to-noise of the car DOAS zenith-sky  
24 measurements and consequently larger errors in the  $\text{NO}_2$  DSCDs. Nevertheless, the high correlation  
25 coefficient of the linear relationship ( $R = 0.94$ ) is promising, in particular when thinking of  
26 applying this method to  $\text{NO}_2$   $\text{VCD}_{\text{tropo}}$  obtained from long-term MAX-DOAS measurements,  
27 which provide better statistics.

28

#### 29 **4.4 Path-averaged $\text{NO}_2$ mixing ratios**





1 Although the  $\text{NO}_2/\text{O}_4$  ratio gives an overall impression of spatiotemporal changes of  $\text{NO}_2$  amounts  
2 over Vienna, an absolute quantification of  $\text{NO}_2$  amounts (e.g. the conversion into mixing ratios) is  
3 not possible with this approach. Therefore, another method is used for the estimation of path-  
4 averaged  $\text{NO}_2$  mixing ratios at 160 m altitude of the rotating tower platform (see Sect. 3.7.2).

5 Estimated horizontal optical path lengths as a function of the azimuthal viewing direction obtained  
6 from measurements taken on 29 April (blue) and 9 May (red) 2016 are shown in Fig. 16. Both  
7 curves represent the last round measurements recorded during those days, when the reference  
8 zenith-sky measurement was taken shortly afterwards. Overall, higher hOPLs are observed on 9  
9 May, which was a day with wind speeds reaching up to  $15 \text{ km h}^{-1}$ . The exceptionally low wind  
10 speeds observed on 29 April ( $< 5 \text{ km h}^{-1}$ ) explain the lower values of hOPL on that day. Low values  
11 of hOPL are generally linked to low visibility, which is the result of an increased aerosol  
12 accumulation over emission hot spots on that otherwise cloudless day. As aerosols largely affect  
13 hOPL under such conditions (Sinreich et al., 2013), it is reasonable that lowest values (5-6 km) are  
14 preferably found in off-axis directions between Eastern and Southern directions, which include  
15 areas with high traffic roads and industry. In contrast, highest hOPLs are observed in the North of  
16 the Vienna Danube Tower on both days (10-11 km). This is reasonable because those regions are  
17 known as rather rural areas without significant emission sources. The highest hOPLs estimated in  
18 our study are slightly lower than the mean value (12.9 km) reported in Seyler et al. (2017), but still  
19 within the standard deviation.

20 Although our assumption made on the limitation of the horizontal light path length towards the hill  
21 might be critical, we argue that the distance of 6.95 km between the Vienna Danube Tower and the  
22 summit of that hill is still lower than  $12.9 \pm 4.5 \text{ km}$  and thus seems to be optimal for this  
23 normalization approach.

24 Estimated path-averaged  $\text{NO}_2$  mixing ratios are shown for 29 April (blue) and 9 May (red) 2016 in  
25 Fig. 17. Again, only the last rotations of those days are presented in the graph. As expected from  
26 the observed wind conditions and estimated hOPLs, path-averaged  $X_{\text{NO}_2}$  is higher on 29 April.  
27 Over rural areas, which are located in the North of the Vienna Danube Tower, values are lowest  
28 (2.5 to 4 ppb) on both days. In contrast, highest values (up to 9 ppb) are again observed towards



1 SE. We note that path-averaged mixing ratios are only shown for two tower rotations, which took  
2 place shortly before noon – at a time when the peak in NO<sub>2</sub> amounts over the city is past.

3 For a better illustration, X<sub>NO<sub>2</sub></sub> as a function of hOPL obtained from the last rotation of tower DOAS  
4 off-axis measurements and X<sub>NO<sub>2</sub></sub> values calculated from simultaneous in situ measurements are  
5 plotted on a geographical map in Fig. 18 for 29 April (left) and 9 May 2016 (right). We note that  
6 the NO<sub>2</sub> mixing ratios estimated from tower DOAS off-axis measurements are averages over  
7 several kilometers at 160 m above ground, whereas NO<sub>2</sub> mixing ratios from in situ stations rather  
8 represent point measurements at the surface level. The comparison therefore implies that the  
9 variability of NO<sub>2</sub> as observed at 160 m above ground is much less pronounced than that between  
10 the individual ground stations. Moreover, horizontal gradients in 160 m above ground are small.  
11 As already outlined above, highest NO<sub>2</sub> amounts obtained from both measurements are generally  
12 found over the city center and over high traffic roads in the Southeast of the city center on 29 April,  
13 a day with very low wind speeds (< 5 km h<sup>-1</sup>). The picture looks different for 9 May, when wind  
14 was blowing from Southeast and wind speeds reached values of up to 15 km h<sup>-1</sup>. Highest NO<sub>2</sub>  
15 amounts from tower DOAS off-axis observations are found in parallel to the wind direction in this  
16 case. On both days, NO<sub>2</sub> mixing ratios are about a factor four larger at the surface level when  
17 compared with path-averaged values at 160 m above, which is in good agreement with the 25%  
18 reported in Dieudonne et al. (2013), who compared surface concentrations with in situ  
19 concentrations at 300 m above ground in Paris.

20

## 21 **5 Summary and outlook**

22 In this case study, unique ground-based remote sensing measurements have been coupled with  
23 surface in situ measurements to investigate the NO<sub>2</sub> distributions in the planetary boundary layer  
24 in the Viennese metropolitan area.

25 A DOAS instrument was used for the determination of the spatial and temporal NO<sub>2</sub> distributions  
26 in and around the urban area of Vienna. The instrument was applied in two different measurement  
27 setups: Car DOAS zenith-sky and tower DOAS off-axis. The former DOAS-type approach, which  
28 is already well established and documented in the literature, was used for a total of twenty identical



1 car journeys, which were carried out on nine days in April, September, October, and November  
2 2015 during the morning hours. The latter configuration is innovative in the sense that horizontal  
3 measurements for more than 100 azimuthal angles are possible within a 360° rotation and within  
4 less than half an hour. The latter setup was used for collecting more than thirty rotations of spectral  
5 measurements on five days in April and May 2016.

6 A DOAS fitting procedure, based on recommendations made for the CINDI-2 campaign  
7 ([www.tropomi.eu/data-products/cindi-2](http://www.tropomi.eu/data-products/cindi-2)), is applied to the collected spectral measurements to  
8 retrieve NO<sub>2</sub> DSCDs. Overall, good fit quality is found for both DOAS-type measurements, in  
9 particular when NO<sub>2</sub> amounts were high.

10 As the car DOAS zenith-sky measurements include a contribution from both the background and  
11 stratospheric NO<sub>2</sub>, a correction scheme based on measurements and chemical transport model  
12 simulations is applied. The subsequent conversion of NO<sub>2</sub> DSCDs into NO<sub>2</sub> VCD<sub>tropo</sub> is performed  
13 by applying stratospheric and tropospheric AMFs as derived from radiative transfer calculations.

14 In order to correct light path lengths in the troposphere, NO<sub>2</sub> DSCDs obtained from tower DOAS  
15 off-axis observations are normalized with O<sub>4</sub> DSCDs in a first step. In a second step, the assumption  
16 that the Kahlenberg (484 m a.s.l) limits the horizontal optical light path length at an azimuth angle  
17 of 305° is made. The distance between the Vienna Danube Tower and the summit of Kahlenberg  
18 (6.95 km) is then used for the normalization of O<sub>4</sub> DSCDs to obtain horizontal optical path lengths  
19 (hOPLs).

20 By analyzing NO<sub>2</sub> DSCDs at high temporal resolution along the individual car journeys,  
21 characteristic horizontal NO<sub>2</sub> changes as a function of distance could be derived. While the absolute  
22 differences between the first and consecutive measurements increases sharply over the first two  
23 kilometers (by a factor of 1.5 to 4), the observed increase clearly weakens during the remaining  
24 kilometers. From this observation we conclude, that 1-2 km is a characteristic scale of the NO<sub>2</sub>  
25 fields observed in Vienna during the morning hours.

26 The analysis of NO<sub>2</sub> VCD<sub>tropo</sub> from car DOAS zenith-sky and DSCD NO<sub>2</sub>/O<sub>4</sub> from tower DOAS  
27 off-axis measurements opened up interesting insights into the spatial and temporal variations of  
28 NO<sub>2</sub>. The results imply that wind speed and wind direction impact strongly on the NO<sub>2</sub> distributions



1 in Vienna. By using data on wind speed and wind direction from several stations within the  
2 metropolitan area of Vienna, short-scale NO<sub>2</sub> transport events could be identified.

3 The comparison of VCD<sub>tropo</sub> from car DOAS zenith-sky measurements with in situ NO<sub>2</sub>  
4 concentrations, which is based on the conversion of both quantities into mixing ratios of NO<sub>2</sub>,  
5 revealed good linear correlation for days when the wind was blowing from the Southeast (R = 0.72-  
6 0.94). In contrast, weak correlation was found for days when the wind was blowing from the  
7 Northwest (R < 0.33), which might be related to the relative location of air masses affected by  
8 dense traffic to the selected in situ monitoring stations.

9 Depending on wind conditions, lap averages of near-surface NO<sub>2</sub> mixing ratios (XNO<sub>2</sub>) estimated  
10 from car DOAS zenith-sky measurements applying a linear regression analysis are in the range of  
11 3.8 to 26.2 ppb and in good agreement with XNO<sub>2</sub> obtained from in situ measurements.

12 Taking into account all the assumptions that have been made for the conversion of DSCDs into  
13 VCD<sub>tropo</sub> and also for the subsequent translation of VCD<sub>tropo</sub> into XNO<sub>2</sub>, the method to derive near-  
14 surface mixing ratios seems to work well – at least for the lap averages considered in this study.

15 The estimation of hOPL and XNO<sub>2</sub> from the tower DOAS off-axis measurements revealed  
16 interesting insights into an upper layer of the PBL, although only few measurements are presented  
17 due to the lack of sequential zenith-sky measurements that could be taken as reference. Overall,  
18 NO<sub>2</sub> mixing ratios are about a factor four larger at the surface level when compared with path-  
19 averaged values at 160 m above. The path-averaged mixing ratios are about 35% smaller at 160 m  
20 above ground, when qualitatively compared to XNO<sub>2</sub> from car DOAS zenith-sky measurements  
21 performed on days with similar wind conditions.

22 Although the NO<sub>2</sub> hourly European maximum dose rate was not exceeded when measurements  
23 were taken, NO<sub>2</sub> amounts in the urban environment of Vienna are substantial, in particular during  
24 morning hours and when wind speeds are low.

25 We note that the idea of performing tower DOAS off-axis measurements was born when car DOAS  
26 zenith-sky measurements were already taken. Due to other priorities and limited manpower at the  
27 time when tower DOAS off-axis measurements were recorded, car DOAS zenith-sky



1 measurements could not be carried out simultaneously. For future campaigns in Vienna, however,  
2 simultaneous measurements of the two DOAS configurations should be taken into consideration.

3 Future efforts will be made to test the linear regression analysis on measurements from three static  
4 MAX-DOAS instruments, which are located in Vienna as part of the VINDOBONA (VIenna  
5 horizontal and vertical Distribution OBServations Of Nitrogen dioxide and Aerosols) project  
6 ([www.doas-vindobona.at](http://www.doas-vindobona.at)). Once the method is mature and optimized, it could also be applied to  
7 satellite measurements of  $VCD_{\text{tropo}}$ . This would help to obtain near-surface mixing ratios of  $\text{NO}_2$   
8 from the integrated column amounts on a global scale.

9 Additional car DOAS zenith-sky and tower DOAS off-axis measurements that complement the  
10 operational performance of the two MAX-DOAS instruments are also foreseen in the future.  
11 Taking these measurements and also data from the relatively large number of air quality monitoring  
12 stations into consideration, Vienna can be seen as an optimal urban location for future satellite  
13 validation campaigns.

14

## 15 **Acknowledgements**

16 This study was funded by the University of Bremen and the Austrian Science Fund (FWF): I 2296-  
17 N29. We like to thank “Amt der Niederösterreichischen Landesregierung“ and “Amt der Wiener  
18 Landesregierung“ for making the air quality data freely available. We wish to acknowledge the  
19 provision of meteorological data by the Austrian official weather service (ZAMG). Christoph  
20 Lotteraner and Martin Piringer (ZAMG) are acknowledged for calculating time-series of mixing-  
21 height at Wien/Hohe Warte. We thank Andreas Hilboll (MARUM-Bremen) for the provision of  
22 simulated stratospheric  $\text{NO}_2$  amounts. Last but not least, we want to thank Mario Meyer and the  
23 staff from the Vienna Danube Tower for giving us the opportunity to perform experimental  
24 measurements from the rotating Café and for providing technical assistance.

25

## 26 **References**



- 1 Anderson, G., Clough, S., Kneizys, F., Chetwynd, J., and Shettle, E.: AFGL atmospheric  
2 constituent profiles (0–120 km), Tech. Rep. AFGL-TR-86-0110, Air Force Geophys. Lab.,  
3 Hanscom Air Force Base, Bedford, Mass., 1986.
- 4 Chipperfield, M. P.: Multiannual simulations with a three-dimensional chemical transport model,  
5 J. Geophys. Res., 104, 1781–1805, 1999.
- 6 Constantin, D. E., Merlaud, A., Van Roozendael, M., Voiculescu, M., Fayt, C., Hendrick, F.,  
7 Pinardi, G., and Georgescu, L.: Measurements of tropospheric NO<sub>2</sub> in Romania using a zenith–  
8 sky mobile DOAS system and comparisons with satellite observations, Sensors, 13, 3922–3940,  
9 2013.
- 10 Danckert, T., Fayt, C., Van Roozendael, M., De Smedt, I., Letocart, V., Merlaud, A., and Pinardi,  
11 G.: QDOAS Software, 2015.
- 12 Dee, D. P., Uppala, S. M., Simmons, A. J., Berrisford, P., Poli, P., Kobayashi, S., Andrae, U.,  
13 Balmaseda, M. A., Balsamo, G., Bauer, P., Bechtold, P., Beljaars, A. C. M., van de Berg, L., Bidlot,  
14 J., Bormann, N., Delsol, C., Dragani, R., Fuentes, M., Geer, A. J., Haimberger, L., Healy, S. B.,  
15 Hersbach, H., Hólm, E. V., Isaksen, L., Kållberg, P., Köhler, M., Matricardi, M., McNally, A. P.,  
16 Monge-Sanz, B. M., Morcrette, J.-J., Park, B.-K., Peubey, C., de Rosnay, P., Tavolato, C., Thépaut,  
17 J.-N., and Vitart, F.: The ERA-Interim reanalysis: configuration and performance of the data  
18 assimilation system, Q. J. Roy. Meteorol. Soc., 137, 553–597, doi:10.1002/qj.828, 2011.
- 19 Dieudonné, E., Ravetta, F., Pelon, J., Goutail, F., and Pommereau, J.-P.: Linking NO<sub>2</sub> surface  
20 concentration and integrated content in the urban developed atmospheric boundary layer, Geophys.  
21 Res. Lett., 40, 1247–1251, doi:10.1002/grl.50242, 2013.
- 22 Dockery, D. W., Pope, A., Xu, X., Spengler, J. D., Ware, J. H., Fay, M., E., Ferris, B. J., and  
23 Speizer, F. E.: An association between air pollution and mortality in six U.S. cities, New England  
24 Journal of Medicine, 329, 1753–1759, 1993.
- 25 Dragomir, C. M., Constantin, D.-E., Voiculescu, M., Georgescu, L. P., Merlaud, A., and van  
26 Roozendael, M.: Modeling results of atmospheric dispersion of NO<sub>2</sub> in an urban area using METI–



- 1 LIS and comparison with coincident mobile DOAS measurements, Atmospheric Pollution  
2 Research 6, 503-510, 2015.
- 3 Fontjin, A., Sabadell, A. J., and Ronco, R. J.: Homogeneous chemiluminescence measurement of  
4 nitric oxide with ozone, Anal. Chem., 42, 575–579, 1970.
- 5 Frins, E., Bobrowski, N., Osorio, M., Casaballe, N., Belsterli, G., Wagner, T., and Platt, U.:  
6 Scanning and mobile multi-axis DOAS measurements of SO<sub>2</sub> and NO<sub>2</sub> emissions from an electric  
7 power plant in Montevideo, Uruguay, Atmos. Environ. 98, 347-356,  
8 doi:10.1016/j.atmosenv.2014.03.069, 2014.
- 9 Gomez, L., Navarro-Comas, M., Puentedura, O., Gonzalez, Y., Cuevas, E., and Gil-Ojeda, M.:  
10 Long-path averaged mixing ratios of O<sub>3</sub> and NO<sub>2</sub> in the free troposphere from mountain MAX-  
11 DOAS, Atmos. Meas. Tech., 7, 3373-3386, <https://doi.org/10.5194/amt-7-3373-2014>, 2014.
- 12 Hermans, C., Vandaele, A., Carleer, M., Fally, S., Colin, R., Jenouvrier, A., Coquart, B., and  
13 Mérianne, M.-F.: Absorption cross-sections of atmospheric constituents: NO<sub>2</sub>, O<sub>2</sub>, and H<sub>2</sub>O,  
14 Environ. Sci. Pollut. Res., 6, 151–158, doi:10.1007/BF02987620, 1999.
- 15 Heue, K.-P., Richter, A., Bruns, M., Burrows, J. P., v. Friedeburg, C., Platt, U., Pundt, I., Wang, P.,  
16 and Wagner, T.: Validation of SCIAMACHY tropospheric NO<sub>2</sub>-columns with AMAXDOAS  
17 measurements, Atmos. Chem. Phys., 5, 1039–1051, doi:10.5194/acp-5-1039-2005, 2005.
- 18 Hilboll, A., Richter, A., and Burrows, J. P.: Long-term changes of tropospheric NO<sub>2</sub> over  
19 megacities derived from multiple satellite instruments, Atmos. Chem. Phys., 13, 4145-4169,  
20 doi:10.5194/acp-13-4145-2013, 2013.
- 21 Hong, Q., Liu, C., Chan, K. L., Hu, Q., Xie, Z., Liu, H., Si, F., and Liu, J.: Ship-based MAX-DOAS  
22 measurements of tropospheric NO<sub>2</sub>, SO<sub>2</sub>, and HCHO distribution along the Yangtze River, Atmos.  
23 Chem. Phys., 18, 5931-5951, <https://doi.org/10.5194/acp-18-5931-2018>, 2018.
- 24 Hönninger, G., von Friedeburg, C., and Platt, U.: Multi axis differential optical absorption  
25 spectroscopy (MAX-DOAS), Atmos. Chem. Phys., 4, 231–254, doi:10.5194/acp-4-231-2004,  
26 2004.



- 1 Ibrahim, O., Shaiganfar, R., Sinreich, R., Stein, T., Platt, U., and Wagner, T.: Car MAX-DOAS  
2 measurements around entire cities: quantification of NO<sub>x</sub> emissions from the cities of Mannheim  
3 and Ludwigshafen (Germany), *Atmos. Meas. Tech.*, 3, 709-721, doi:10.5194/amt-3-709-2010,  
4 2010.
- 5 Ionov, D. and Poberovskii, A.: Quantification of NO<sub>x</sub> emission from St Petersburg (Russia) using  
6 mobile DOAS measurements around the entire city, *International Journal of Remote Sensing*, 36:9,  
7 2486-2502, DOI: 10.1080/01431161.2015.1042123, 2015.
- 8 IPCC: Climate Change 2013: The Physical Science Basis, contribution of Working Group I to the  
9 Fifth Assessment Report of the Intergovernmental Panel on Climate Change, edited by: Stocker,  
10 T. F., Qin, D., Plattner, G.-K., Tignor, M., Allen, S. K., Boschung, J., Nauels, A., Xia, Y., Bex, V.,  
11 and Midgley, P. M., Cambridge Univ. Press, Cambridge, UK and New York, NY, USA, 2013.
- 12 Johansson, M., Galle, B., Yu, T., Tang, L., Chen, D., Li, H., Li, J. X., and Zhang, Y.: Quantification  
13 20 of total emission of air pollutants from Beijing using mobile mini-DOAS, *Atmos. Environ.* 42,  
14 6926–6933, 2008.
- 15 Johansson, M., Rivera, C., de Foy, B., Lei, W., Song, J., Zhang, Y., Galle, B., and Molina, L.:  
16 Mobile mini-DOAS measurement of the emission of NO<sub>2</sub> and HCHO from Mexico City, *Atmos.*  
17 *Chem. Phys. Discuss.*, 9, 865–882, 2009.
- 18 Johansson, M., Rivera, C., de Foy, B., Lei, W., Song, J., Zhang, Y., Galle, B., and Molina,  
19 L.: Mobile mini-DOAS measurement of the emission of NO<sub>2</sub> and HCHO from Mexico City,  
20 *Atmos. Chem. Phys. Discuss.*, 9, 865–882, 2009.
- 21 Knepp, T., Pippin, M., Crawford, J., Chen, G., Szykman, J., Long, R., Cowen, L., Cede, A.,  
22 Abuhassan, N., Herman, J., Delgado, R., Compton, J., Berkoff, T., Fishman, J., Martins, D.,  
23 Stauffer, R., Thompson, A. M., Weinheimer, A., Knapp, D., Montzka, D., Lenschow, D.,  
24 and Neil, D.: Estimating surface NO<sub>2</sub> and SO<sub>2</sub> mixing ratios from fast-response total column  
25 observations and potential application to geostationary missions, *J. Atmos. Chem.*, D15308,  
26 doi:10.1007/s10874-013-9257-6, 2013.





- 1 Kramer, L. J., Leigh, R. J., Remedios, J. J., and Monks, P. S.: Comparison of OMI and ground-  
2 based in situ and MAX-DOAS measurements of tropospheric nitrogen dioxide in an urban area, *J.*  
3 *Geophys. Res.*, 113, D16S39, doi:10.1029/2007JD009168, 2008.
- 4 Künzli, N., Kaiser, R., Medina, S., Studnicka, M., Chanel, O., Filliger, P., Herry, M., Horak Jr, F.,  
5 Puybonnieux-Textier, V., Quénel, P., Schneider, J., Seethaler, R., Vergnaud, J. C., and Sommer,  
6 H.: Public-health impact of outdoor and traffic-related air pollution: A European assessment,  
7 *Lancet*, 356, 795–801, 2000.
- 8 Kurucz, R. L., Furenhild, I., Brault, J., and Testermann, L.: Solar flux atlas from 296 to 1300 nm,  
9 *National Solar Observatory Atlas No. 1*, June 1984, 1984.
- 10 Lee, D. S., Köhler, I., Grobler, E., Rohrer, F., Sausen, R., Gallardo- Klenner, L., Olivier, J. G. J.,  
11 Dentener, F. J., and Bouwman, A. F.: Estimations of global NO(x) emissions and their  
12 uncertainties, *Atmos. Environ.*, 31, 1735–1749, 1997.
- 13 Lotteraner, C. and Piringer, M.: Mixing-Height Time Series from Operational Ceilometer  
14 Aerosol-Layer Heights, *Bound.-Lay. Meteorol.*, 161, 265–287, [https://doi.org/10.1007/s10546-](https://doi.org/10.1007/s10546-016-0169-2)  
15 [016-0169-2](https://doi.org/10.1007/s10546-016-0169-2), 2016.
- 16 Meier, A. C., Schönhardt, A., Bösch, T., Richter, A., Seyler, A., Ruhtz, T., Constantin, D.-E.,  
17 Shaiganfar, R., Wagner, T., Merlaud, A., Van Roozendael, M., Belegante, L., Nicolae, D.,  
18 Georgescu, L., and Burrows, J. P.: High-resolution airborne imaging DOAS measurements of NO<sub>2</sub>  
19 above Bucharest during AROMAT, *Atmos. Meas. Tech.*, 10, 1831-1857,  
20 <https://doi.org/10.5194/amt-10-1831-2017>, 2017.
- 21 Merlaud, A., Tack, F., Constantin, D., Georgescu, L., Maes, J., Fayt, C., Mingireanu, F.,  
22 Schuettmeyer, D., Meier, A. C., Schönardt, A., Ruhtz, T., Bellegante, L., Nicolae, D., Den Hoed,  
23 M., Allaart, M., and Van Roozendael, M.: The Small Whiskbroom Imager for atmospheric  
24 composition monitorinG (SWING) and its operations from an unmanned aerial vehicle (UAV)  
25 during the AROMAT campaign, *Atmos. Meas. Tech.*, 11, 551-567, [https://doi.org/10.5194/amt-](https://doi.org/10.5194/amt-11-551-2018)  
26 [11-551-2018](https://doi.org/10.5194/amt-11-551-2018), 2018.



- 1 Nowlan, C. R., Liu, X., Janz, S. J., Kowalewski, M. G., Chance, K., Follette-Cook, M. B., Fried,  
2 A., González Abad, G., Herman, J. R., Judd, L. M., Kwon, H.-A., Loughner, C. P., Pickering, K.  
3 E., Richter, D., Spinei, E., Walega, J., Weibring, P., and Weinheimer, A. J.: Nitrogen dioxide and  
4 formaldehyde measurements from the GEOstationary Coastal and Air Pollution Events (GEO-  
5 CAPE) Airborne Simulator over Houston, Texas, Atmos. Meas. Tech. Discuss.,  
6 <https://doi.org/10.5194/amt-2018-156>, in review, 2018.
- 7 Ortega, I., Koenig, T., Sinreich, R., Thomson, D., and Volkamer, R.: The CU 2-D-MAX-DOAS  
8 instrument – Part 1: Retrieval of 3-D distributions of NO<sub>2</sub> and azimuth-dependent OVOC ratios,  
9 Atmos. Meas. Tech., 8, 2371-2395, <https://doi.org/10.5194/amt-8-2371-2015>, 2015.
- 10 Perner, D. and Platt, U.: Detection of nitrous acid in the atmosphere by differential optical  
11 absorption, Geophys. Res. Lett., 6, 917–920, 1979.
- 12 Peters, E., Wittrock, F., Großmann, K., Frieß, U., Richter, A., and Burrows, J. P.: Formaldehyde  
13 and nitrogen dioxide over the remote western Pacific Ocean: SCIAMACHY and GOME-2  
14 validation using ship-based MAX-DOAS observations, Atmospheric Chemistry and Physics, 12,  
15 11179-11197, 2012.
- 16 Platt, U. and Stutz, J.: Differential Optical Absorption Spectroscopy. Physics of Earth and Space  
17 Environments, Springer, Berlin, 2008.
- 18 Richter, A., Burrows, J. P., Nüß, H., Granier, C., and Niemeier, U.: Increase in tropospheric  
19 nitrogen dioxide over China observed from space, Nature, 437, 129-132, DOI:  
20 10.1038/nature04092, 2005.
- 21 Richter, A., Begoin, M., Hilboll, A., and Burrows, J. P.: An improved NO<sub>2</sub> retrieval for the GOME-  
22 2 satellite instrument, Atmos. Meas. Tech., 4, 1147-1159, doi:10.5194/amt-4-1147-2011, 2011.
- 23 Rivera, C., Sosa, G., Whrnschimmel, H., de Foy, B., Johansson, M., and Galle, B.: Tula  
24 industrial complex (Mexico) emissions of SO<sub>2</sub> and NO<sub>2</sub> during the MCMA 2006 field campaign  
25 using a mobile mini-DOAS system, Atmos. Chem. Phys., 9, 6351–6361, doi:10.5194/acp-9-6351-  
26 2009, 2009.



- 1 Rivera, C., Barrera, H., Grutter, M., Zavala, M., Galle, B., Bei, N., Li, G., and Molina, L. T.: NO<sub>2</sub>  
2 fluxes from Tijuana using a mobile mini-DOAS during Cal-Mex 2010, *Atmos. Environ.*, 70, 532-  
3 539, 2013.
- 4 Roscoe, H. K., Van Roozendaal, M., Fayt, C., du Piesanie, A., Abuhassan, N., Adams, C., Akrami,  
5 M., Cede, A., Chong, J., Clémer, K., Friess, U., Gil Ojeda, M., Goutail, F., Graves, R., Griesfeller,  
6 A., Grossmann, K., Hemerijckx, G., Hendrick, F., Herman, J., Hermans, C., Irie, H., Johnston, P.  
7 V., Kanaya, Y., Kreher, K., Leigh, R., Merlaud, A., Mount, G. H., Navarro, M., Oetjen, H.,  
8 Pazmino, A., Perez-Camacho, M., Peters, E., Pinardi, G., Puentedura, O., Richter, A., Schönhardt,  
9 A., Shaiganfar, R., Spinei, E., Strong, K., Takashima, H., Vlemmix, T., Vrekoussis, M., Wagner,  
10 T., Wittrock, F., Yela, M., Yilmaz, S., Boersma, F., Hains, J., Kroon, M., Píters, A., and Kim, Y.  
11 J.: Intercomparison of slant column measurements of NO<sub>2</sub> and O<sub>4</sub> by MAX-DOAS and zenith-sky  
12 UV and visible spectrometers, *Atmos. Meas. Tech.*, 3, 1629-1646, doi:10.5194/amt-3-1629-2010,  
13 2010.
- 14 Rothman, L. S., Barbe, A., Benner, D. C., Brown, L. R., Camy-Peyret, C., Carleer, M. R., Chance,  
15 K., Clerbaux, C., Dana, V., Devi, V. M., Fayt, A., Flaud, J.-M., Gamache, R. R., Goldman, A.,  
16 Jacquemart, D., Jucks, K. W., Lafferty, W. J., Mandin, J.-Y., Massie, S. T., Nemtchinov, V.,  
17 Newnham, D. A., Perrin, A., Rinsland, C. P., Schroeder, J., Smith, K. M., Smith, M. A. H., Tang,  
18 K., Toth, R. A., Auwera, J. V., Varanasi, P., and Yoshino, K.: The HITRAN molecular  
19 spectroscopic database: edition of 2000 including updates through 2001, *J. Quant. Spectr. Rad.*  
20 *Transf.*, 82, 5–44, 2003.
- 21 Rozanov, V., Rozanov, A., Kokhanovsky, A., and Burrows, J.: Radiative transfer through  
22 terrestrial atmosphere and ocean: Software package SCIATRAN, *J. Quant. Spec. R.*  
23 *Trans.*, doi: 10.1016/j.jqsrt.2013.07.004, 2014.
- 24 Schönhardt, A., Altube, P., Gerilowski, K., Krautwurst, S., Hartmann, J., Meier, A. C., Richter, A.,  
25 and Burrows, J. P.: A wide field-of-view imaging DOAS instrument for two-dimensional trace gas  
26 mapping from aircraft, *Atmos. Meas. Tech.*, 8, 5113-5131, doi:10.5194/amt-8-5113-2015, 2015.



- 1 Schreier, S. F., Peters, E., Richter, A., Lampel, J., Wittrock, F., and Burrows, J. P.: Ship-based  
2 MAX-DOAS measurements of tropospheric NO<sub>2</sub> and SO<sub>2</sub> in the South China and Sulu Sea,  
3 Atmos. Environ., 102, 331–343, doi:10.1016/j.atmosenv.2014.12.015, 2015.
- 4 Schreier, S. F., Richter, A., Wittrock, F., and Burrows, J. P.: Estimates of free-tropospheric NO<sub>2</sub>  
5 and HCHO mixing ratios derived from high-altitude mountain MAX-DOAS observations at  
6 midlatitudes and in the tropics, Atmos. Chem. Phys., 16, 2803–2817, [https://doi.org/10.5194/acp-](https://doi.org/10.5194/acp-16-2803-2016)  
7 16-2803-2016, 2016.
- 8 Serdyuchenko, A., Gorshelev, V., Weber, M., Chehade, W., and Burrows, J. P.: High spectral  
9 resolution ozone absorption cross-sections – Part 2: Temperature dependence, Atmos. Meas. Tech.,  
10 7, 625–636, doi:10.5194/amt-7-625-2014, 2014.
- 11 Seyler, A., Wittrock, F., Kattner, L., Mathieu-Üffing, B., Peters, E., Richter, A., Schmolke, S., and  
12 Burrows, J. P.: Monitoring shipping emissions in the German Bight using MAX-DOAS  
13 measurements, Atmos. Chem. Phys., 17, 10997–11023, [https://doi.org/10.5194/acp-17-10997-](https://doi.org/10.5194/acp-17-10997-2017)  
14 2017, 2017.
- 15 Shaiganfar, R., Beirle, S., Sharma, M., Chauhan, A., Singh, R. P., and Wagner, T.: Estimation of  
16 NO<sub>x</sub> emissions from Delhi using Car MAX-DOAS observations and comparison with OMI  
17 satellite data, Atmos. Chem. Phys., 11, 10871–10887, doi:10.5194/acp-11-10871-2011, 2011.
- 18 Sinnhuber, B.-M., Weber, M., Amankwah, A., and Burrows, J. P.: Total ozone during the unusual  
19 Antarctic winter of 2002, Geophys. Res. Lett., 30, 1580–1584, doi:10.1029/2002GL016798,  
20 2003a.
- 21 Sinnhuber, M., Burrows, J. P., Chipperfield, M. P., Jackman, C. H., Kallenrode, M.-B., Künzi, K.  
22 F., and Quack, M.: A model study of the impact of magnetic field structure on atmospheric  
23 composition during solar proton events, Geophys. Res. Lett., 30, 1818–1821,  
24 doi:10.1029/2003GL017265, 2003b.
- 25 Sinreich, R., Merten, A., Molina, L., and Volkamer, R.: Parameterizing radiative transfer to  
26 convert MAX-DOAS dSCDs into near-surface box-averaged mixing ratios, Atmos. Meas. Tech.,  
27 6, 1521–1532, <https://doi.org/10.5194/amt-6-1521-2013>, 2013.



- 1 Spangl, W. and Nagl, C.: Jahresbericht der Luftgütemessungen in Österreich 2015, REPORT REP-  
2 0562, Umweltbundesamt GmbH, Wien, 2016.
- 3 Tack, F., Merlaud, A., Iordache, M.-D., Danckaert, T., Yu, H., Fayt, C., Meuleman, K., Deutsch,  
4 F., Fierens, F., and Van Roozendael, M.: High-resolution mapping of the NO<sub>2</sub> spatial distribution  
5 over Belgian urban areas based on airborne APEX remote sensing, *Atmos. Meas. Tech.*, 10, 1665-  
6 1688, <https://doi.org/10.5194/amt-10-1665-2017>, 2017.
- 7 Takashima, H., Irie, H., Kanaya, Y., and Syamsudin, F.: NO<sub>2</sub> observations over the western Pacific  
8 and Indian Ocean by MAX-DOAS on Kaiyo, a Japanese research vessel, *Atmospheric  
9 Measurement Techniques*, 5, 2351-2360, 2012.
- 10 Thalman, R. and Volkamer, R.: Temperature dependent absorption cross-sections of O<sub>2</sub>-O<sub>2</sub>  
11 collision pairs between 340 and 630 nm and at atmospherically relevant pressure., *Phys. Chem.  
12 Chem. Phys.*, 15, 15371–15381, <https://doi.org/10.1039/c3cp50968k>, 2013.
- 13 Vandaele, A. C., Hermans, C., Simon, P. C., Roozendael, M. V., Guilmot, J. M., Carleer, M., and  
14 Colin, R.: Fourier transform measurement of NO<sub>2</sub> absorption cross-section in the visible range at  
15 room temperature, *J. Atmos. Chem.*, 25, 289–305, 1996.
- 16 Wagner, T., Ibrahim, O., Shaiganfar, R., and Platt, U.: Mobile MAX-DOAS observations of  
17 tropospheric trace gases, *Atmos. Meas. Tech.*, 3, 129-140, doi:10.5194/amt-3-129-2010, 2010.
- 18 Wang, P., Richter, A., Bruns, M., Rozanov, V. V., Burrows, J. P., Heue, K.-P., Wagner, T., Pundt,  
19 I., and Platt, U.: Measurements of tropospheric NO<sub>2</sub> with an airborne multi-axis DOAS instrument,  
20 *Atmos. Chem. Phys.*, 5, 337–343, doi:10.5194/acp-5-337-2005, 2005.
- 21 Wang, S., Zhou, B., Wang, Z., Yang, S., Hao, N., Valks, P., Trautmann, T., and Chen, L.: Remote  
22 Sensing of NO<sub>2</sub> Emission from the Central Urban Area of Shanghai (China) Using the Mobile  
23 DOAS Technique. *Journal of Geophysical Research*, 117 (D13305), doi:10.1029/2011JD016983,  
24 2012.
- 25 WHO: Health Aspects of Air Pollution with Particulate Matter, Ozone and Nitrogen Dioxide,  
26 World Health Organization, Bonn, 2003.



- 1 Winkler, H., Sinnhuber, M., Notholt, J., Kallenrode, M.-B., Steinhilber, F., Vogt, J., Zieger, B.,  
2 Glassmeier, K.-H., and Stadelmann, A.: Modeling impacts of geomagnetic field variations on  
3 middle atmospheric ozone responses to solar proton events on long timescales, *J. Geophys. Res.*,  
4 113, 11 pp., D02302, doi:10.1029/2007JD008574, 2008.
- 5 Wittrock, F., Oetjen, H., Richter, A., Fietkau, S., Medeke, T., Rozanov, A., and Burrows, J. P.:  
6 MAX-DOAS measurements of atmospheric trace gases in Ny-Ålesund – Radiative transfer studies  
7 and their application, *Atmos. Chem. Phys.*, 4, 955–966, doi:10.5194/acp-4-955-2004, 2004.
- 8 Wu, F. C., Xie, P. H., Li, A., Chan, K. L., Hartl, A., Wang, Y., Si, F. Q., Zeng, Y., Qin, M., Xu, J.,  
9 Liu, J. G., Liu, W. Q., and Wenig, M.: Observations of SO<sub>2</sub> and NO<sub>2</sub> by mobile DOAS in the  
10 Guangzhou eastern area during the Asian Games 2010, *Atmos. Meas. Tech.*, 6, 2277–2292,  
11 doi:10.5194/amt-6-2277-2013, 2013.
- 12 [www.doas-vindobona.at](http://www.doas-vindobona.at)
- 13 [www.donauturm.at](http://www.donauturm.at)
- 14 [www.statistik.at](http://www.statistik.at)
- 15 [www.tropomi.eu/data-products/cindi-2](http://www.tropomi.eu/data-products/cindi-2)
- 16 [www.vcoe.at](http://www.vcoe.at)
- 17
- 18
- 19
- 20
- 21
- 22
- 23

1 **Table 1.** DOAS settings for the retrieval of NO<sub>2</sub>.

<b>Fit parameter</b>		<b>Selection/Source</b>
Spectral range		425-490 nm
Polynomial degree		5 (car zenith-sky), 7 (tower off-axis)
Wavelength calibration		Solar atlas (Kurucz et al., 1984)
Reference		Zenith-sky spectrum (close to noontime)
<b>Cross section</b>	<b>Temperature</b>	<b>Data source</b>
O <sub>3</sub>	223 K	Serdyuchenko et al. (2014) with I <sub>0</sub> correction
NO <sub>2</sub>	298 K	Vandaele et al. (1996) with I <sub>0</sub> correction
O <sub>4</sub>	293 K	Thalman and Volkamer (2013)
H <sub>2</sub> O	-	Rothmann et al. (2010)
Ring	-	QDOAS (Danckert et al., 2015)

2

3

4

5

6

7

8

9

10

11

12

13

14

15



1 **Table 2.** Summary of statistics of the individual car journeys including lap averages of wind speed,  
 2 wind direction, temperature, pressure, number density of air, mixing-height, in-situ NO<sub>2</sub> from  
 3 selected air quality monitoring stations, and NO<sub>2</sub> VCD<sub>tropo</sub> from car DOAS measurements.  
 4 Converted averaged NO<sub>2</sub> mixing ratios for both measurements are also given. The correlation  
 5 coefficients (R) obtained from the linear relationship between car DOAS and in situ NO<sub>2</sub> are also  
 6 shown (further details are given in the text).

	10.04.2015 <sup>a</sup>			27.09.2015 <sup>b</sup>		28.09.2015 <sup>b</sup>	
Car journey (UT)	05:27-06:59	07:06-08:35	08:40-10:04	07:11-08:42	08:42-10:17	06:36-08:20	08:21-10:05
Wind speed [km h <sup>-1</sup> ] <sup>d</sup>	3.9±2.4	5.4±2.8	6.7±2.4	14.4±4.9	15.3±5.4	16.1±5	19.8±6.4
Wind direction [deg] <sup>d</sup>	135.5±29.6	126.2±29.3	114.1±24.6	337.2±7.1	240.3±81.5	187.1±114.2	91.7±99.4
Temperature [°C] <sup>e</sup>	7.4±1	10.4±0.8	13±0.7	12.6±0.3	13.7±0.4	12.4±0.6	14.2±0.5
Pressure [hPa] <sup>e</sup>	994.6±0.1	994.7±0	994.5±0	996.1±0.3	996.5±0.1	1000.6±0.2	1000.7±0.1
Number density of air [molec cm <sup>-3</sup> ] <sup>f</sup>	2.568e+19	2.541e+19	2.517e+19	2.525e+19	2.516e+19	2.538e+19	2.522e+19
Mixing-height [m] <sup>g</sup>	148.2±28.6	311.7±46.4	445.7±30.1	1103.7±50.2	1045.4±30	541.3±105.9	1161.1±209.7
In situ NO <sub>2</sub> [µg m <sup>-3</sup> ] <sup>h</sup>	63.3±22.9	43.7±23	35.5±20.3	9.3±5.2	8.4±4.5	20.4±11.7	15.4±10.2
In situ X <sub>NO<sub>2</sub></sub> [ppb] <sup>i</sup>	31.6±11.4	22.0±11.6	18.1±10.3	4.7±2.7	4.3±2.3	10.3±5.9	7.8±5.2
Car DOAS NO <sub>2</sub> [10 <sup>16</sup> molec cm <sup>-2</sup> ] <sup>j</sup>	1.34±0.49	1.02±0.49	0.91±0.74	0.23±0.09	0.15±0.09	0.42±0.18	0.33±0.28
Car DOAS (BL) X <sub>NO<sub>2</sub></sub> [ppb] <sup>k</sup>	35.2±12.9	12.9±6.2	8.1±6.6	0.8±0.3	0.6±0.4	3±1.3	1.1±0.9
Car DOAS (Surface) X <sub>NO<sub>2</sub></sub> [ppb] <sup>l</sup>	26.2	21.5	18	7.3	6.5	11	3.8
Correlation coefficient <sup>m</sup>		0.80		0.37		0.65	

7

8 **Table 2.** continued.

	02.10.2015 <sup>b</sup>			06.10.2015 <sup>b</sup>		19.10.2015 <sup>c</sup>	
Car journey (UT)	05:22-06:58	07:01-08:29	08:29-09:55	06:57-08:23	08:24-09:57	06:57-08:30	08:32-09:56
Wind speed [km h <sup>-1</sup> ] <sup>d</sup>	4.7±2.1	10.9±2.9	16.9±4.5	8.1±3.3	10±3.1	8.1±2.9	11±2.6
Wind direction [deg] <sup>d</sup>	125.3±40.3	134.8±6.9	139.8±5.8	120.4±7.7	122.8±11.6	293.3±23.4	312.8±7.1
Temperature [°C] <sup>e</sup>	7.7±1.3	11.1±1.2	14.8±0.9	12.9±1	14.7±0.2	7.7±0.2	8.1±0.1
Pressure [hPa] <sup>e</sup>	997.6±0.1	997.5±0	997±0.2	982±0	981.9±0.1	987±0.1	986.8±0
Number density of air [molec cm <sup>-3</sup> ] <sup>f</sup>	2.573e+19	2.542e+19	2.508e+19	2.471e+19	2.486e+19	2.545e+19	2.541e+19
Mixing-height [m] <sup>g</sup>	206.8±51.6	350.4±44.5	666.9±136.2	381.6±24.8	480.4±34.4	412.4±23.2	374.5±19.1
In situ NO <sub>2</sub> [µg m <sup>-3</sup> ] <sup>h</sup>	44.1±17.3	27.2±10	19.9±12.6	27.3±9	25.4±10.2	30.8±10.9	30.4±10
In situ X <sub>NO<sub>2</sub></sub> [ppb] <sup>i</sup>	22±8.6	13.7±5	10.1±6.4	14.1±4.6	13.2±5.3	15.5±5.5	15.3±5.1
Car DOAS NO <sub>2</sub> [10 <sup>16</sup> molec cm <sup>-2</sup> ] <sup>j</sup>	0.74±0.48	0.47±0.35	0.24±0.2	0.65±0.41	0.55±0.37	0.53±0.35	0.5±0.21
Car DOAS (BL) X <sub>NO<sub>2</sub></sub> [ppb] <sup>k</sup>	13.9±9	5.3±3.9	1.5±1.2	6.8±4.2	4.5±3.1	5.1±3.4	5.2±2.2
Car DOAS (Surface) X <sub>NO<sub>2</sub></sub> [ppb] <sup>l</sup>	23.4	16	7.1	13.7	12.2	17.6	15.7
Correlation coefficient <sup>m</sup>		0.73		0.78		0.23	

9



1 **Table 2.** continued.

	23.10.2015 <sup>c</sup>		27.10.2015 <sup>c</sup>		03.11.2015 <sup>c</sup>	
Car journey (UT)	06:58-08:46	08:47-10:14	06:58-08:37	08:37-10:02	06:44-08:15	08:15-09:43
Wind speed [km h <sup>-1</sup> ] <sup>d</sup>	13.8±4	14±4.2	16±5	19±5.2	8.2±3.2	9.9±3.7
Wind direction [deg] <sup>d</sup>	282.6±8	294.5±9.5	134±7.2	137.1±6.7	152.1±31	157.2±20.9
Temperature [°C] <sup>e</sup>	10±0.3	11.1±0.4	9±0.2	10.6±1	3±0.4	4.2±0.4
Pressure [hPa] <sup>e</sup>	991.3±0.4	992±0.1	991.6±0.1	991.7±0.1	995.7±0.1	995.4±0.1
Number density of air [molec cm <sup>-3</sup> ] <sup>f</sup>	2.536e+19	2.528e+19	2.545e+19	2.531e+19	2.611e+19	2.599e+19
Mixing-height [m] <sup>g</sup>	357.5±24.1	482.3±50	460±14.7	631.2±79.7	417.4±8.1	471.2±25.7
In situ NO <sub>2</sub> [µg m <sup>-3</sup> ] <sup>h</sup>	26.3±8.2	25.4±7.9	22.8±10.3	18.8±8.6	52.7±19.6	36.6±18.2
In situ X <sub>NO<sub>2</sub></sub> [ppb] <sup>i</sup>	13.3±4.2	12.8±4	11.5±5.2	9.5±4.3	25.9±9.6	18.1±9
Car DOAS NO <sub>2</sub> [10 <sup>16</sup> molec cm <sup>-2</sup> ] <sup>j</sup>	1.41±0.5	1±0.51	0.27±0.15	0.23±0.14	0.88±0.51	0.72±0.47
Car DOAS (BL) X <sub>NO<sub>2</sub></sub> [ppb] <sup>k</sup>	15.5±5.5	8.2±4.1	2.3±1.3	1.5±0.9	8±4.6	5.9±3.8
Car DOAS (Surface) X <sub>NO<sub>2</sub></sub> [ppb] <sup>l</sup>	17.1	14.3	11.5	7.4	23.3	20.3
Correlation coefficient <sup>m</sup>	0.07		0.72		0.94	

2

3

<sup>a</sup>Reference measurement taken on 10 April 2015 at 10:49 UT (48° 17' 52.08'' N, 16° 33' 44.64'' E).

4

<sup>b</sup>Reference measurement taken on 27 September 2015 at 10:17 UT (48° 21' 52.75'' N, 16° 31' 20.24'' E).

5

<sup>c</sup>Reference measurement taken on 23 October 2015 at 10:14 UT (48° 21' 53.85'' N, 16° 31' 22.48'' E).

6

<sup>d</sup>Measurements from 9 stations are provided by ZAMG. Values represent lap averages and standard deviations.

7

<sup>e</sup>Measurements provided by the BOKU weather station. Values represent lap averages and standard deviations.

8

<sup>f</sup>Calculations are based on the relationship between pressure and temperature measurements. Values represent lap averages.

9

<sup>g</sup>Measurements provided by ZAMG. Values represent lap averages and standard deviations.

10

<sup>h</sup>Measurements from 15 stations provided by UBA. Values represent lap averages and standard deviations.

11

<sup>i</sup>Conversion of mass concentrations into mixing ratios is based on Eq. 5.

12

<sup>j</sup>Conversion of DSCD<sub>meas</sub> into VCD<sub>trope</sub> is based on Eq. 1.

13

<sup>k</sup>Conversion of VCD<sub>trope</sub> into boundary layer mixing ratios is based on Eq. 3.

14

<sup>l</sup>Conversion of VCD<sub>trope</sub> into surface mixing ratios is based on Eq. 4.

15

<sup>m</sup>Values represent correlation coefficients between in situ NO<sub>2</sub> [ppb] and Car DOAS (BL) NO<sub>2</sub> [ppb].

16

17

18

19

20

21

22



- 1 **Table 3.** Overview on selected air quality monitoring stations, operated by the Environment Agency Austria.
- 2

Lower Austria								
	Klosterneuburg (Wiener Straße)	Klosterneuburg (Wiesentgasse)	Mannswörth (Danubiastraße)	Schwechat	Vösendorf	Wolkersdorf	Gänserndorf	
Latitudes	48° 18' 25'' N	48° 18' 10'' N	48° 08' 42'' N	48° 08' 45'' N	48° 07' 32'' N	48° 23' 32'' N	48° 20' 05'' N	
Longitudes	16° 19' 35'' E	16° 19' 17'' E	16° 30' 40'' E	16° 28' 37'' E	16° 19' 60'' E	16° 31' 20'' E	16° 43' 50'' E	
Vienna								
	A23 (Wehlistraße)	Belgradplatz	Floridsdorf	Kaiserebersdorf	Laer Berg	Liesing	Lobau	Stadlau
Latitudes	48° 11' 05'' N	48° 10' 30'' N	48° 15' 42'' N	48° 09' 26'' N	48° 09' 41'' N	48° 08' 17'' N	48° 09' 45'' N	48° 13' 37'' N
Longitudes	16° 24' 28'' E	16° 21' 45'' E	16° 23' 53'' E	16° 28' 38'' E	16° 23' 39'' E	16° 17' 48'' E	16° 31' 36'' E	16° 27' 35'' E

3

4

5

6

7

8

9

10

11

12

13

14

15

16



- 1 **Table 4.** Overview on selected meteorological stations, operated by the Austrian official weather  
2 service.

Lower Austria					
	Brunn am Gebirge	Gänsersdorf	Gross-Enzersdorf	Wolkersdorf	
	(Stadt)				
Latitudes	48° 06' 25'' N	48° 20' 16'' N	48° 11' 59'' N	48° 22' 49'' N	
Longitudes	16° 16' 12'' E	16° 42' 49'' E	16° 33' 33'' E	16° 30' 27'' E	
Vienna					
	Donaufeld	Hohe Warte	Innere Stadt	Stammersdorf	Unterlaa
Latitudes	48° 15' 27'' N	48° 14' 55'' N	48° 11' 54'' N	48° 18' 21'' N	48° 07' 30'' N
Longitudes	16° 26' 00'' E	16° 21' 23'' E	16° 22' 01'' E	16° 24' 20'' E	16° 25' 10'' E

3

4

5

6

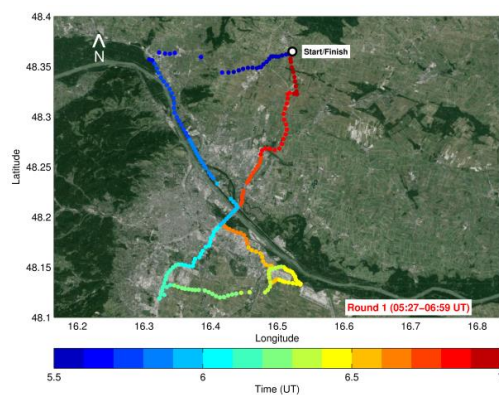
7

8

9

10

11



1

2 **Figure 1.** An example of a single car journey as performed on 10 April 2015 between 05:27 and  
3 06:59 UT.

4

5

6

7

8

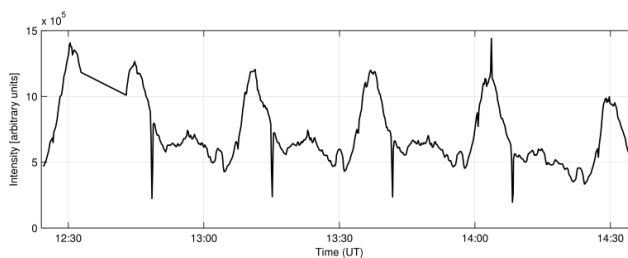
9

10

11

12

13



1

2 **Figure 2.** An example of a time series of the intensity of the spectrum as measured with the  
3 DOAS instrument from the rotating tower platform on 22 April 2016 between 12:25 and 14:35  
4 UT. The sharp dips indicate a decrease in intensity due to pointing towards a skyscraper, which  
5 blocks the view of the instruments.

6

7

8

9

10

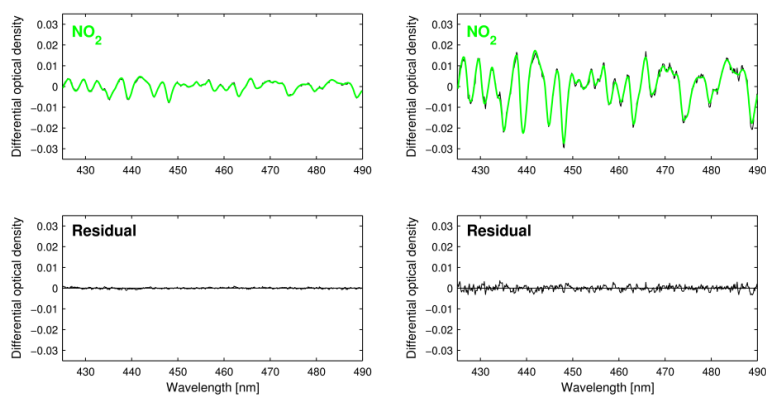
11

12

13

14

15



1

2 **Figure 3.** Exemplary fit results from the DOAS analysis in the 425-490 nm fitting window for a  
3 car DOAS spectrum (left panels), as measured on 10 April 2015 (SZA = 47.68°, DSCD = 4.03 x  
4 10<sup>16</sup> molec cm<sup>-2</sup>) and for a tower DOAS spectrum (right panels), as measured on 29 April 2016  
5 (SZA = 66.99°, DSCD = 1.46 x 10<sup>17</sup> molec cm<sup>-2</sup>).

6

7

8

9

10

11

12

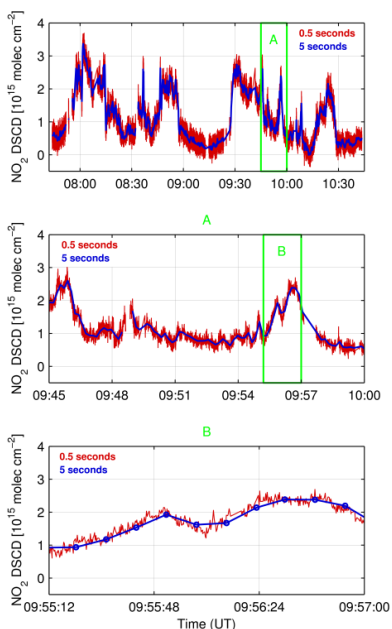
13

14

15

16

17



1

2 **Figure 4.** Temporal resolution of NO<sub>2</sub> DSCDs based on the car DOAS zenith-sky measurements  
 3 performed on 3 November 2015. The red and blue lines show data at a resolution of 0.5 and 5  
 4 seconds, respectively. The upper panel shows the NO<sub>2</sub> DSCDs for the whole period of  
 5 observations of that day, whereas the middle and lower panels represent shorter time sections for  
 6 clarity.

7

8

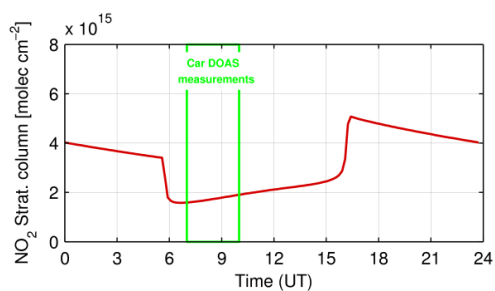
9

10

11

12

13



1

2 **Figure 5.** Stratospheric NO<sub>2</sub> above Vienna on 19 October 2014 (red line) as obtained from the  
3 Bremen 3d chemistry transport model (B3dCTM). The green rectangle indicates the time period  
4 of car DOAS measurements performed on that day.

5

6

7

8

9

10

11

12

13

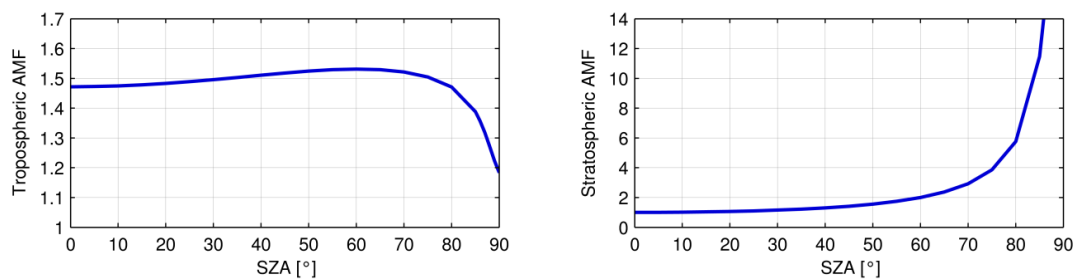
14

15

16

17





1

2 **Figure 6.** Computed AMFs as a function of solar zenith angle for the troposphere (left) and  
3 stratosphere (right).

4

5

6

7

8

9

10

11

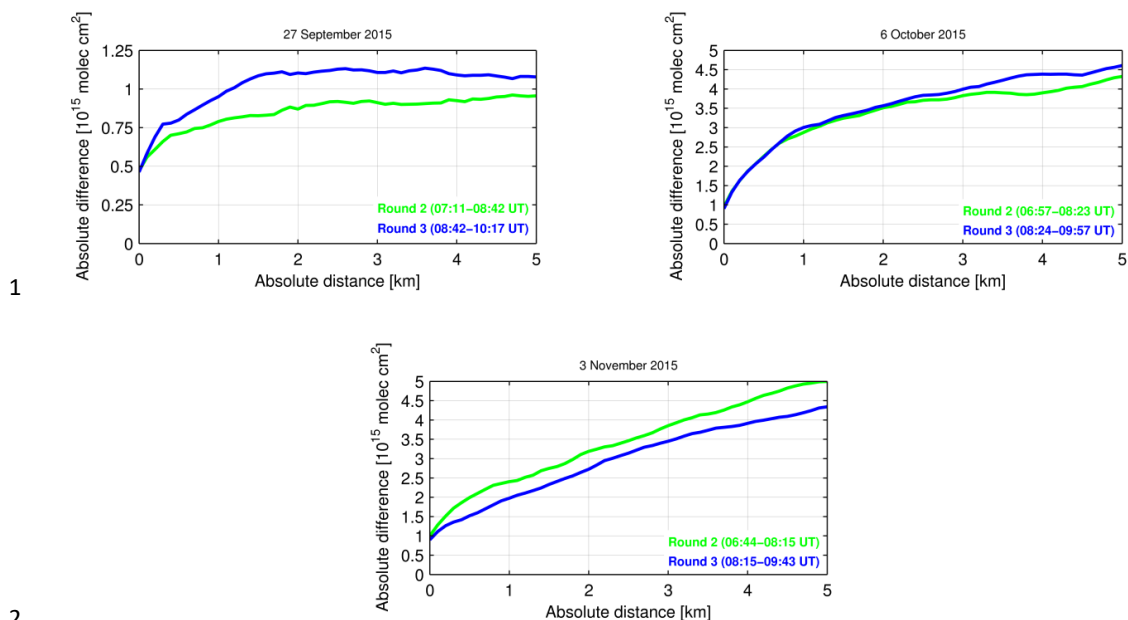
12

13

14

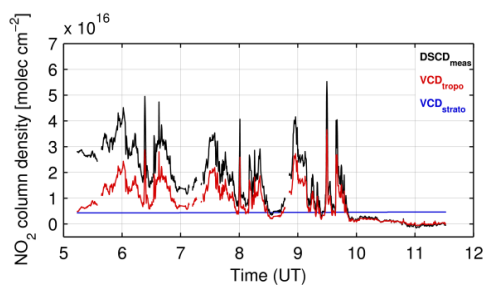
15

16



3 **Figure 7.** Mean absolute difference in  $\text{NO}_2$  DSCDs as a function of the absolute distance (see  
4 Sect. 3.2.1) for car DOAS zenith-sky measurements performed on three selected days with  
5 different wind conditions and  $\text{NO}_2$  levels.

6  
7  
8  
9  
10  
11  
12  
13  
14



1

2 **Figure 8.** Time series of NO<sub>2</sub> DSCD<sub>meas</sub> (black), VCD<sub>tropo</sub> (red), and VCD<sub>strato</sub> (blue) obtained  
3 from car DOAS zenith-sky spectra recorded on 10 April 2015.

4

5

6

7

8

9

10

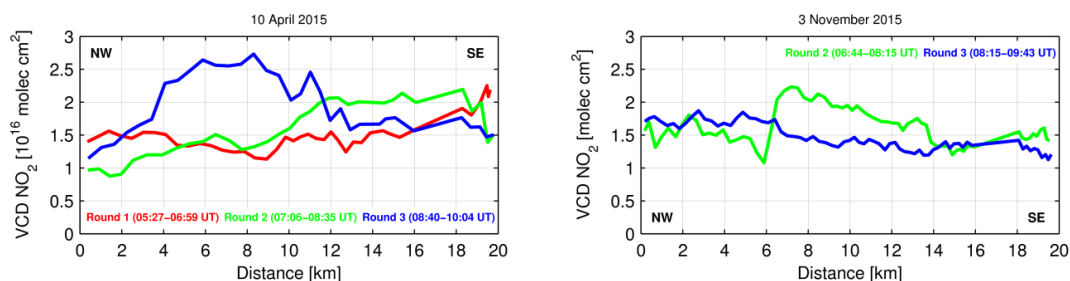
11

12

13

14

15



1

2 **Figure 9.** Temporal evolution of tropospheric NO<sub>2</sub> for the car DOAS zenith-sky measurements as  
3 performed on 10 April and 3 November 2015. The red, green, and blue curves represent NO<sub>2</sub>  
4 VCD<sub>tropo</sub> as obtained along the A22 during the first, second, and third journey, respectively.

5

6

7

8

9

10

11

12

13

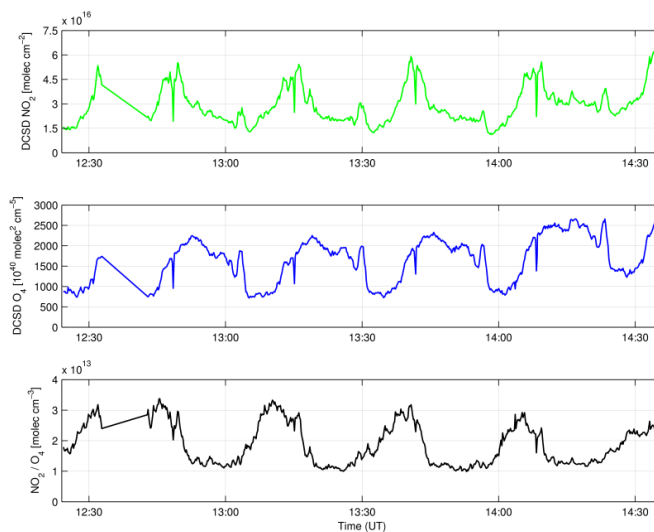
14

15

16

17

18



1

2 **Figure 10.** Time series of NO<sub>2</sub> (upper) and O<sub>4</sub> (middle) DSCDs as obtained from the tower  
3 DOAS off-axis measurements performed on 22 April 2016. The ratio of NO<sub>2</sub>/O<sub>4</sub> is shown in the  
4 lowest panel.

5

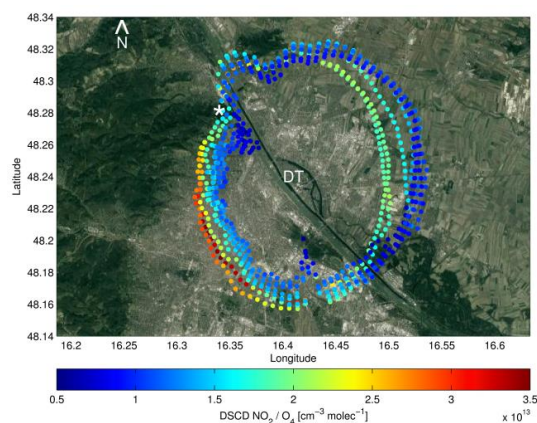
6

7

8

9

10



1

2 **Figure 11.** Spatial and temporal variability of the NO<sub>2</sub>/O<sub>4</sub> ratio (here, the radius is determined by  
 3 DSCD O<sub>4</sub> values) on 10 May 2016 between 05:57 and 09:56 UT observed by tower DOAS off-  
 4 axis measurements. The position of the Vienna Danube Tower (DT) is highlighted in the center  
 5 of the geographical map. The white asterisk represents the summit of Kahlenberg (484 m a.s.l),  
 6 which is used for the estimation of horizontal optical path lengths.

7

8

9

10

11

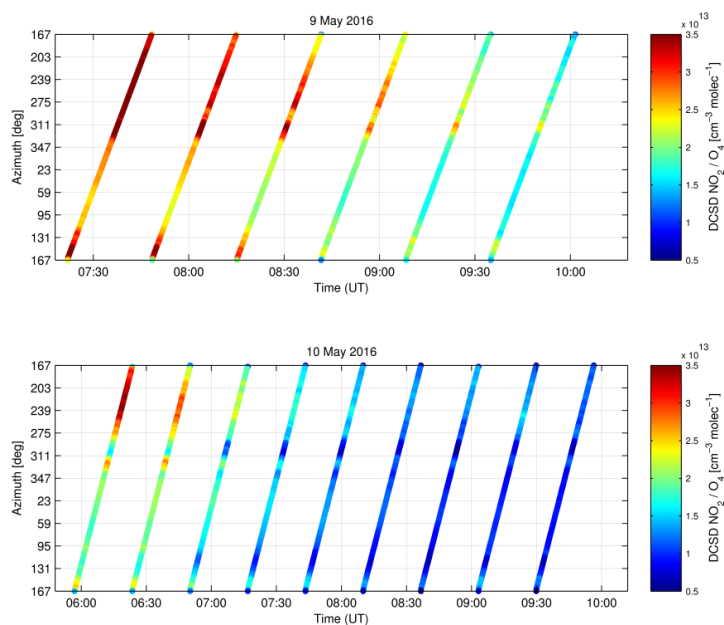
12

13

14

15

16



1

2

3 **Figure 12.** Spatial and temporal variability of DSCD NO<sub>2</sub>/O<sub>4</sub> obtained from tower DOAS off-  
4 axis measurements performed on 9 and 10 May 2016.

5

6

7

8

9

10

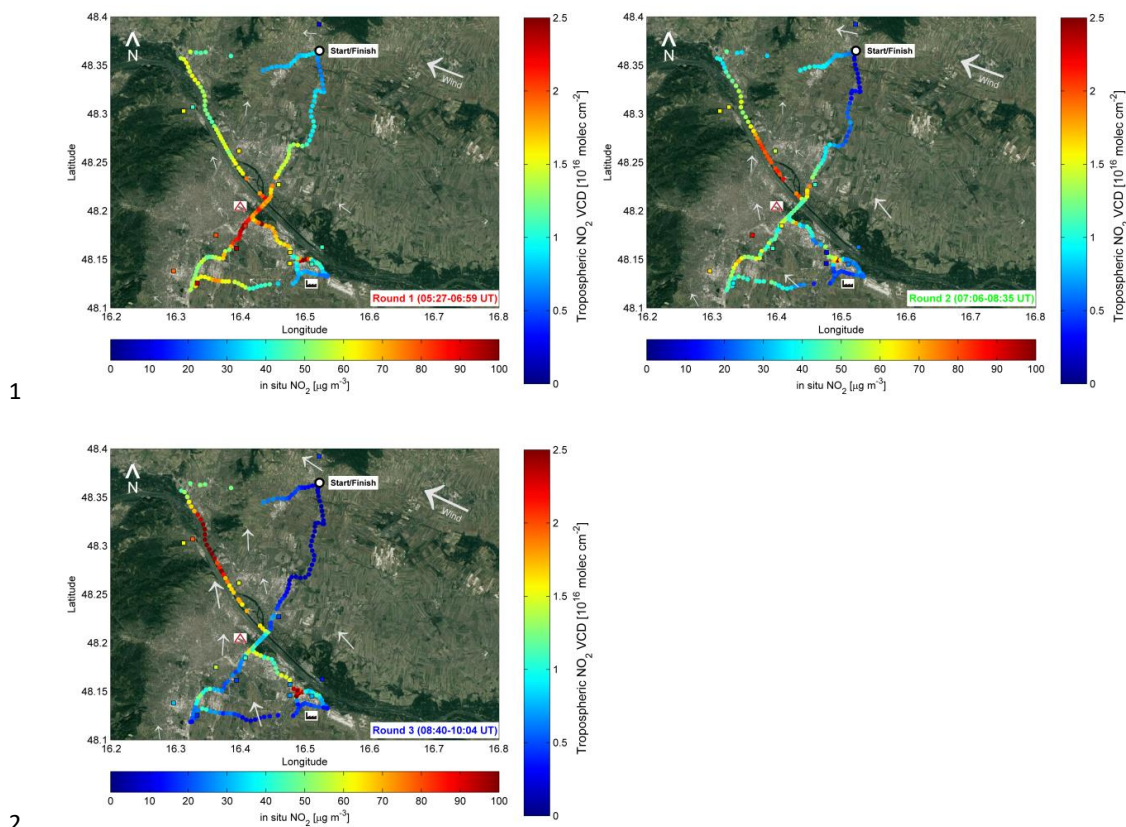
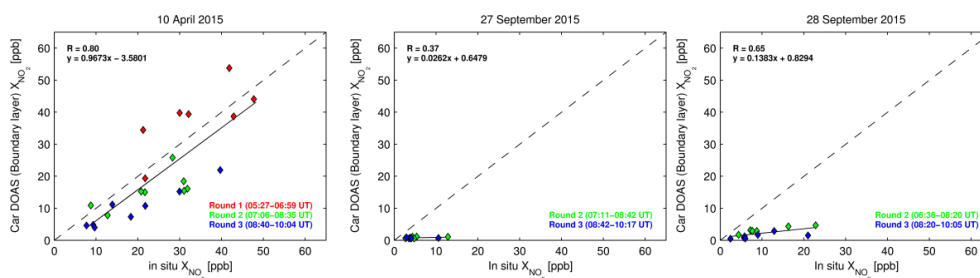


**Figure 13.** Spatial and temporal evolution of  $\text{NO}_2$  on 10 April 2015 in Vienna as measured by the car DOAS zenith-sky (dots) and in situ surface measurements (squares). Wind direction and wind speed obtained from local weather stations are indicated by white arrows. The size of the arrows is weighted by the corresponding averaged wind speed (2 m above ground) obtained from the individual weather stations. Averaged wind speeds over the course of the car DOAS zenith-sky measurements taken on this day ranged between 2.28 and 12.81  $\text{km h}^{-1}$ .

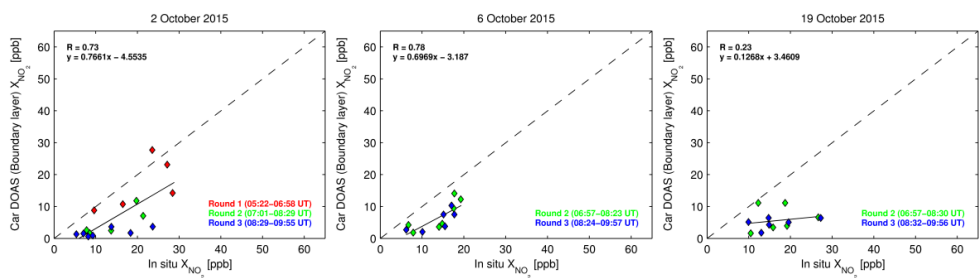




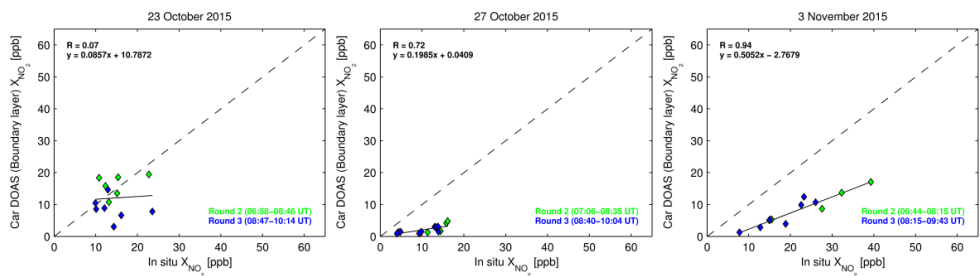
1



2



3



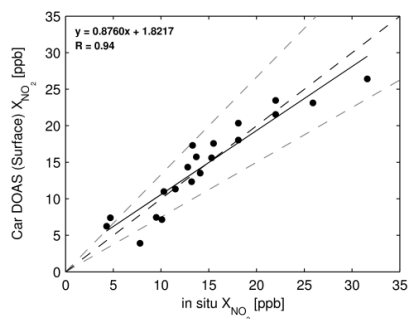
4 **Figure 14.** Comparison of boundary layer NO<sub>2</sub> mixing ratios estimated from car DOAS zenith-  
 5 sky measurements with NO<sub>2</sub> mixing ratios obtained from in situ measurements on the nine days  
 6 when measurements were performed. The dotted line represents the 1:1 relationship.

7

8

9

10



1

2 **Figure 15.** Comparison of lap averaged near-surface  $NO_2$  mixing ratios estimated from car  
 3 DOAS zenith-sky measurements with  $NO_2$  mixing ratios obtained from in situ measurements.  
 4 Lap averages of all twenty performed car rides are included in the calculation. The black and grey  
 5 dotted lines represent the 1:1 relationship and  $\pm 25\%$ , respectively.

6

7

8

9

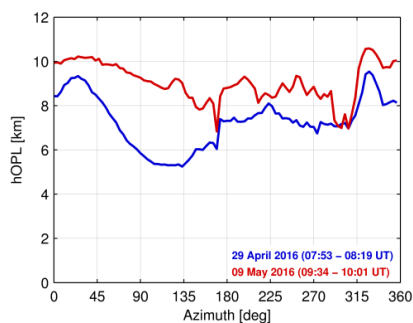
10

11

12

13

14



1

2 **Figure 16.** Estimated horizontal optical path length obtained from tower DOAS off-axis  
3 measurements recorded during two tower platform rotations on 29 April and 9 May 2016.

4

5

6

7

8

9

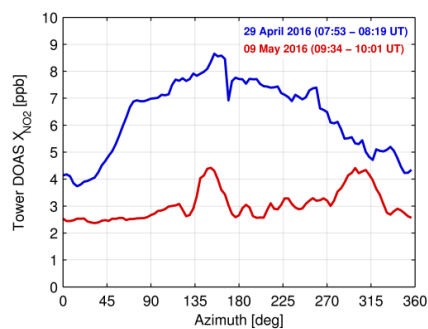
10

11

12

13

14



1

2 **Figure 17.** Estimated path-averaged NO<sub>2</sub> mixing ratios obtained from tower DOAS off-axis  
3 measurements recorded during two tower platform rotations on 29 April and 9 May 2016.

4

5

6

7

8

9

10

11

12

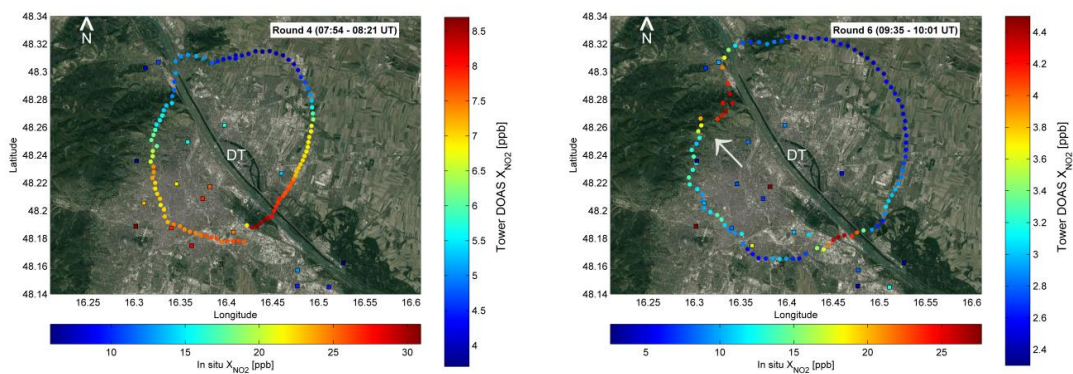
13

14

15

16

17



1

2 **Figure 18.** Spatial variability of  $X_{\text{NO}_2}$  in Vienna based on tower DOAS off-axis (dots) and in situ  
3 surface measurements (squares) obtained on 29 April and 9 May 2016.